Exp Brain Res (2009) 198:59–83
DOI 10.1007/s00221-009-1936-9

RESEARCH ARTICLE

EEG coherence: topography and frequency structure

David Balin Chorlian · Madhavi Rangaswamy · Bernice Porjesz

Received: 6 August 2008 / Accepted: 29 June 2009 / Published online: 22 July 2009

Abstract Topographical patterns of bipolar EEG coherence are frequency specific, indicating the presence of diverse neuroanatomical and neurophysiological factors in EEG production. Bipolar EEG coherence values were calculated at 50 frequency bins ranging from 3 to 28 Hz for 39 coherence pairs. Data were derived from 4.25 min of resting EEG obtained from 106 healthy adult male subjects and analyzed in 0.5 Hz bins by Fourier transform methods. Frequency bands were clearly separated at 8.5 and 13 Hz, with a less distinct separations at 6 and 20 Hz. Within pair (non-topographic) and across pair (topographic), measures gave similar patterns of separation. Significant pathways were primarily anterior–posterior interhemispheric or perpendicular to the anterior–posterior axis. There was little difference between left and right for comparable pairs. Theta band coherent activity involves distinct midline and temporal sources, with temporal sources showing anterior/posterior differentiation. In contrast, alpha activity has a distinct posterior focus, while beta activity shows no clear global structure. A spatially homogeneous model based on characteristics of thalamocortical connectivity accounts for much of the data, but departures from the model indicate the contribution of other neural factors to coherence.

Keywords Coherence · Bipolar · Topography · EEG

This work was supported by NIAAA Grants AA002686, AA005524, and AA008401 at SUNY Downstate Medical Center.

D. B. Chorlian (✉) · M. Rangaswamy · B. Porjesz
Henri Begleiter Neurodynamics Laboratory,
Department of Psychiatry, SUNY Downstate Medical Center,
450 Clarkson Ave., Brooklyn, NY, USA
e-mail: David.Chorlian@downstate.edu

Introduction

Functional connectivity between different regions of the brain in the resting state has been a recent topic of interest in neurophysiological research. Patterns of resting-state activity are important for understanding intrinsic neural function, and may be significant in shaping responses to stimuli (Hanslmayr et al. 2007; Fox et al. 2007; Raichle and Gusnard 2005). Studies with fMRI show "default-mode" networks: regions which show common temporal patterns of hemodynamic activity in the resting state and whose activity may be attenuated in task situations (Raichle and Snyder 2007; Fox and Raichle 2007; Mantini et al. 2007; Salvador et al. 2005). An additional perspective on resting-state activity is offered by the study of connectivity using measures of EEG coherence. Connectivity is established in fMRI studies by the correlations in hemodynamic activity over time between different brain regions. An analogous pattern in an EEG study would be correlations in amplitude over time between different scalp locations within particular frequency ranges. We consider coherence measures of consistency in phase relations between pairs of locations over time a more sensitive measure of connectivity than correlations in amplitude, since communication between two groups of neurons is a function of the pattern of their oscillatory behavior (Fries 2005; Buzski and Draguhn 2004). Since connectivity patterns and neural function may be specific to the frequency of neural activity (von Stein and Sarnthein 2000), a particular advantage of EEG coherence measures is the ability to assess topographic relations as a function of frequency. Although EEG coherence measures cannot provide the anatomical specificity attainable by the use of fMRI, the high degree of frequential specificity provides a useful complement to those results. If coherent activity is

necessary for functional neural communication, and if functional activation changes hemodynamic activity, then examination of EEG coherence measures may be particularly useful in interpreting the functional aspect of connectivity. We suggest, based on the results presented here, that specific resting-state networks (RSN)/connections found in fMRI studies may be associated with neural activity with distinct coherence spectra.

Coherence is a linear synchronization measure between two signals recorded at different locations. It is a statistical measure of the average agreement in phase difference, weighted by amplitude, between two signals measured over time, and is frequency specific. Coherence values range from 0 to 1, with 1 meaning perfect agreement in phase difference and 0 meaning completely random phase differences. A signal recorded at a single electrode is a function not only of the neural activity directly beneath it, but also of neural activity at more distant locations propagated by electromagnetic fields as mediated by the intervening tissue and other matter. This latter phenomenon is called volume conduction. Volume conduction effects can contribute strongly to coherence measures of "raw" signals, inflating their values and reducing their topographic variability. A number of different data transformations (data preprocessing methods), if performed before the coherence calculation, can reduce volume conduction effects. The Laplacian (or current source density) provides a reference-independent transformation which eliminates most volume conduction effects. Signals transformed to bipolar form by subtractions between adjacent electrodes, which is also a reference-independent transformation, fall between Laplacian and "raw" data, eliminating volume conduction effects from about twice the distance between the two electrodes forming the bipolar pair. However, bipolar coherence values are affected by the orientations of the bipolar pairs because of the intrinsic geometry of the electrode configuration and because of the anisotropy of volume conduction effects (Nunez et al. 1997, 1999, 2001; Srinivasan et al. 1998; Grieve et al. 2003). In any analysis, the choice of methods is the result of balancing the extent and purpose of the results with character of the available data. As Nunez et al. (1997, p. 510) point out, each method of coherence estimation will reveal different aspects of functional connectivity.

A theory of EEG coherence is offered by Robinson (2003, 2005) (Robinson et al. 2003) based on an analysis of the mass character of thalamocortical and corticocortical circuits by continuum methods (David and Friston 2003; Steyn-Ross et al. 2007). This theory uses a dispersive model of neural firing patterns; the equation expressing coherence as a function of distance is parameterized by the values of characteristics of individual neural interconnections (Robinson 2003; equations 4, 22). As a consequence, theoretical coherence values are a relatively simple function of the distance between the coherence pairs (we note that the mechanism in the dispersive model is unrelated to volume conduction).

Robinson's (2003) initial paper attributes coherence to a single spatially homogeneous neurophysiological mechanism. [Subsequent papers allow for spatial non-uniformity: O'Connor and Robinson (2004), Robinson (2005). Ursino and Zavaglia (2007) and Zavaglia et al. (2008) provide models with multiple interacting frequency mechanisms.] Although it is unlikely that all coherent EEG activity can be attributed to a spatially homogeneous and isotropic single dispersive mechanism, Robinson's theory provides a useful starting point for the investigation of coherence, since it accounts for the main features of the observed coherence spectra (see Fig. 1) with more fidelity than other models. We may identify patterns which are not solely a function of simple dispersion by applying Robinson's theory to the coherence data to identify and eliminate the effects of that dispersion on coherence values.

In the present study, we examine and describe in detail the topography and frequency structure of EEG coherence in the resting state. We distinguish three modes of characterizing topography. The primary topographic feature is the pattern of connectivity determined by the magnitude of the coherence values between different locations. In that case, topography is characterized in terms of the orientation and location of the lines connecting one location with another. A second aspect of topography is the locational pattern of the grouping of coherence pairs determined by frequency-specific similarity in relative value. A third aspect of topographic structure is the locational pattern of the grouping of coherence pairs determined by the covariance relations among the values of different coherence pairs at the same frequency. Topographic structures indicate neuroanatomical features of possible sources of coherent EEG activity. Frequency structure, such as banding, is determined by abrupt changes in relative values among coherence pairs with changes in frequency. An additional aspect of frequency structure is determined by the covariance relations between the values at different frequencies for each coherence pair. Banding indicates a separation between different neurophysiological sources of coherent EEG activity. Based upon these features, we attempt to identify distinct complexes of coherent EEG activity, and compare them to analogous complexes obtained from other methods of assessing patterns of neural activity. We caution that the scalp-recorded measures of coherent activity alone do not provide enough information to distinguish between the different possible neuroanatomical/neurophysiological factors responsible for that activity.

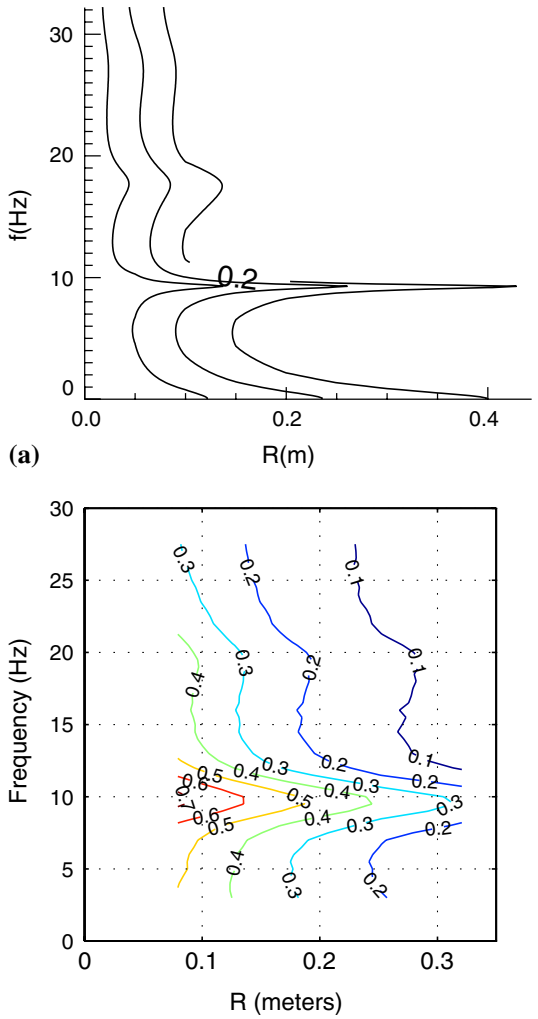

Fig. 1 Comparison of Robinson's theory and observed data. *Upper panel* theoretical isocoherence lines (Robinson 2003; Fig. 2) (isocoherence lines at 0.8, 0.5, 0.2). This figure is reprinted from Robinson (2003), Copyright 2003 Elsevier Publishers. *Lower panel* isocoherence lines estimated from sagittal data. In each case distance is represented on the *X*-axis and frequency on the *Y*-axis

Materials and methods

Participants

The sample consisted of 106 healthy right-handed male volunteers within the age range of 19–47 years (mean age 29.4 years, standard deviation 4.9 years). The participants were recruited through advertisements, and the study was conducted at SUNY Downstate Medical Center at Brooklyn, NY, USA. Individuals with hearing or visual impairment, severe medical problems (e.g., liver diseases, recent surgery and chronic pain conditions), neurological problems (e.g., dementia, delirium, head injury, degenerative diseases and cerebrovascular diseases/conditions), psychiatric illnesses (e.g., schizophrenia, depression, bipolar disorders and other psychoses) or drug/alcohol dependence were excluded from the study. Subjects who had major childhood behavioral disorders, e.g., ADHD (attention deficit hyperactivity disorder), conduct disorder, oppositional defiant disorder and autism were also excluded from the study. Individuals who had a family history of major psychiatric illnesses and those who at the time of the study were on any medication that could affect the central nervous system were also excluded. Subjects with a family history of alcohol/substance dependence were not included in this study. The data of those individuals with severe cognitive deficits based on their score on the mini mental state examination (MMSE) were not used for this study. Experimental procedures were approved by the institutional review board.

Data recording

Each subject wore a fitted electrode cap (Electro-Cap International Inc., Eaton, OH) using the 19-channel montage as specified according to the 10–20 International system [FP1, FP2, F7, F3, FZ, F4, F8, T7, C3, CZ, C4, T8, P7, P3, PZ, P4, P8, O1, O2]. The nose served as reference and the forehead was the ground electrode. Electrode impedences were always maintained below 5K ohms. The electrooculogram (EOG) was recorded from electrodes placed supraorbitally at the outer canthus of the eye. EEG was recorded from the 19 channels with the subjects seated comfortably in a dimly lit sound-attenuated temperature-regulated booth (Industrial Acoustics Company, Bronx, NY). They were instructed to keep their eyes closed and remain relaxed. Subjects were also cautioned not to fall asleep. Electrical activity was amplified 10,000 times by Sensorium EPA-2 Electrophysiology amplifiers (Charlotte, VT), with a bandpass between 0.02 and 50 Hz and recorded using the Neurodynamics software system (Neurodynamics Laboratory, SUNY Downstate Medical Center) running on Concurrent 5550 computers (Concurrent Computer Corporation, Atlanta, GA). The sampling rate was 256 Hz and the activity was recorded for 4.25 min.

Data reduction

EEG analysis was performed at SUNY Downstate Medical Center. A continuous interval comprising 256 s of EEG data was used for analysis. Offline raw data were subjected to wavelet filtering and reconstruction to eliminate high and low frequencies (Bruce and Gao 1994; Strang and Nguyen 1996). The *s*12 wavelet was used to perform a six-level analysis, and the output signal was reconstructed using levels *d*6 through *d*3. This procedure is roughly equivalent to applying a band-pass filter with a range of 2–64 Hz to the data. Subsequently, eye movements were removed by the use of a frequency domain method developed by Gasser et al.

(1985, 1986). This method subtracts a portion of observed ocular activity from observed EEG to obtain the true EEG, based on the difference between the cross-spectral values of trials with high ocular activity and those with low ocular activity. One-second intervals in which the voltage range exceeded 75 μv were excluded from the subsequent analysis; no subject had fewer than 224 s of data subject to analysis. Visual inspection of corrected data confirmed satisfactory artifact removal characteristics.

In order to improve the localization of our signals, consideration was given to both the Laplacian and bipolar data transformations. In our case, the data we wish to analyze were recorded with too few electrodes to use the Laplacian transform (Wang and Begleiter 1999; Babiloni et al. 1995). A bipolar transformation was used to minimize volume conduction effects, although its use limited the density of the coherence pairs, and limited the coverage in the occipital and frontal areas. This is partially compensated for by the use of both sagittally and laterally oriented pairs for interhemispheric coherence. A comparison (see "Comparison to EEG and MEG studies") of our results with those obtained by Srinivasan (1999) using monopolar and Laplacian derivations shows bipolar derivations to have similar effects as Laplacians. [Although bipolar derivations are not often used in EEG studies, previous published work from our laboratory (Porjesz et al. 2002; Rangaswamy et al. 2002, 2003, 2004; Tang et al. 2007b; Chorlian et al. 2007) used bipolar derivations and Tang et al. (2007a) explicitly compared bipolar to monopolar results, showing that bipolar values had greater topographic variability than did monopolar values.] Since over 4 min of resting EEG data were available for each subject, it was possible to use 1/2 Hz frequency bins in Fourier analysis and obtain relatively narrow confidence intervals for the coherence estimates.

The data were software transformed into 38 bipolar derivations formed by the subtraction of adjacent electrodes in both lateral and sagittal orientations, and analyzed in 254 overlapping 2-second epochs by use of a Fourier transform and windowed using a Hamming function (Hamming 1983) to improve the accuracy of the spectral results (we will use the following terminology: a derivation is a single signal obtained either as the "raw" data from a single electrode or by subtracting the signals at adjacent electrodes to obtain a bipolar derivation. Bipolar derivations are called sagittal when the line joining the two adjacent electrodes has an anterior–posterior direction; lateral when the line joining the two adjacent electrodes is orthogonal to the anterior–posterior direction. A coherence pair is a pair of derivations whose coherence is estimated, and called bipolar or monopolar depending on the kind of derivation used in their estimate. A bipolar coherence pair is called sagittal or lateral depending on the orientation of the two derivations, which is the same in any pair used in this study. Note that in many cases the lines connecting the midpoints of the derivations will be perpendicular to the lines connecting the electrodes. This is the case with all the sagittally oriented derivations; the lines connecting the midpoints are always lateral).

Coherence calculation

The standard coherence calculation,

$$\gamma_{ij}(f) = \frac{|G_{ij}(f)|^2}{G_{ii}(f)G_{jj}(f)}$$

where

$$G_{ij}(f) = \frac{1}{N}\sum_{n} X_{in}(f)X_{jn}(f)^*$$

and X_{in} is the Fourier transform of the signal in channel i at epoch n, and '*' indicates the complex conjugate, was applied to each 0.5 Hz frequency bin. Because of the overlapping intervals, the number of epochs used for calculating confidence intervals for the coherence estimates was set at 127. In the analyses described subsequently, the Fisher Z-transform $y = \tanh^{-1}(x)$ was applied to the coherence values.This serves not only to normalize the distributions of values, but also to reduce the difference in confidence intervals between greater and smaller values. [Where necessary, the inverse function [tanh(x)] was applied to produce coherence values]. Coherence was calculated between all pairs of derivations excluding those which had an electrode in common.

Data selection

Only coherence pairs with a mean value of greater than 0.05 over the entire frequency range were included in the study. This criterion was used to ensure reliable coherence estimates at all frequencies (Bendat and Piersol 1971; Nunez et al. 1997; Wang and Tang 2004), and was verified to provide a 99% confidence level for non-zero coherence by Monte Carlo simulation. This choice permits complete interfrequency comparisons at the cost of losing some topographic detail in the alpha range. None of coherence pairs excluded had large values in any part of the frequency range. Consistent with this criterion, 17 lateral pairs were examined: 6 intrahemispheric which did not involve a midline electrode, 4 intrahemispheric which did involve midline electrodes, 3 interhemispheric with symmetrically placed derivations and 4 interhemispheric with asymmetrically placed derivations. The lines connecting the derivations in these latter pairs crossed diagonally from anterior to posterior and from one hemisphere to the other. Similarly, 22 sagittal pairs were examined: 10 fronto-central pairs to provide an all-pairs analysis of that region, 10

corresponding centro-parietal pairs, and 1 frontal and 1 occipital pair (see Appendix for details). Pairs fell into natural groups differentiated by locational characteristics: anterior or posterior, left or right, central or peripheral, and containing a midline channel or not; and by relational characteristics: symmetric or asymmetric, adjacent or distant, and interhemispheric or intrahemispheric; and their combinations (see Table in Appendix for these groupings). In many cases we performed separate analyses on lateral and sagittal pairs, since there is reason to believe that they are measuring different connective systems in the brain (Hagmann et al. 2008) (see "Topographic structure: correlational similarity"). [Pairs with one lateral and one sagittal derivation show extremely low coherence values, even when the derivations are close.]

Aggregative measures and distance modeling

We calculated the mean coherence for each frequency bin of each of the 39 pairs. The maximum coherence and the frequency at which the maximum occurred for each coherence pair and subject was determined by fitting a quadratic to the maximum value of the measured data and the values at the two adjacent points on either side of the maximum, and using the maximum value of the quadratic and the frequency at which that maximum occurred.

Attempting to account for the effect of distance on coherence values guided by Robinson's theory (Robinson 2003, equation 22, p. 166), we used the following equation to fit the observed data

$$\gamma_{ij}(f) = \mathrm{e}^{-(a(f)+b(f)d(i,j))} + \delta_{ij}(f)$$

where $a(f)$ representing the limiting value when the distance is 0 and $b(f)$ representing the amount of decrease with distance, possibly differing for each frequency, are unknown parameters to be estimated and $d(i, j)$ is the distance between sites i and j, taken here are the distance (along the surface of a sphere) between the midpoints of the arcs joining the electrodes included in each of the bipolar derivations. We estimated $a(f)$ and $b(f)$ separately for the sagittally oriented pairs and for the laterally oriented pairs using mean values of coherence at each frequency for each coherence pair. We note that although in the case of monopolar derivations the coherence at very small separations should very nearly equal 1, making $a(f) = 0$, the value of $a(f)$ is left free to enable a better fit to the data. This does not result in an underestimate of the coherences at the smallest distances as seen in Fig. 2. The residuals, $\delta_{ij}(f)$, which are not error terms, show the relative effects of the location and orientation of the coherence pairs on the coherence values, and are essential to gauging frequency and topographic specific characteristics of coherence).

Covariance measures

We use several methods to assess the covariance structure of the coherence measures, attributing common neurophysiological or neuroanatomical sources to highly correlated measures and the absence of common neurophysiological or neuroanatomical sources to measures with a low degree of correlation. In particular, we wish to assess the degree of similarity of coherence at different frequency bins in single coherence pairs, and in the same frequency bin across two or more coherence pairs. The choice of a metric for correlational similarity is motivated by the fact that perfect linear correlational similarity among subjects would occur when the ratio of any two coherence variables for one individual would be the same as that ratio for any other individual. In visual terms, a scatterplot of one coherence variable against another would lie on a straight line through the origin of the variable space. If the variables lie on a straight line not through the origin in the variable space, then we do not consider them to have perfect correlational similarity. Thus we did not use the correlation coefficient as the measure of similarity, although it was calculated as well. A simple measure of bivariate similarity would be a function of the ratio of the singular values of the singular value decomposition of the data matrix of the two coherence variables. In order to be able to generalize the similarity measure to more than two variables, we calculate the normalized entropy (NE) of the singular values of the data matrix of n variables, and use $1 - \mathrm{NE}$ as our correlational similarity measure (CSM). The normalized entropy of $s_1, \ldots, s_n$ is

$$\mathrm{NE}(s_1, \ldots, s_n) = -\sum_{i=1}^{n} \frac{s_i}{S} \log\left(\frac{s_i}{S}\right) / \log(n)$$

where $S = \sum_{i=1}^{n} s_i$. The normalized entropy lies between 0 and 1, and is a maximum where $s_1 = s_2 = \cdots = s_n$ and a minimum where $S = s_1$ and $s_2 = \cdots = s_n = 0$. In order to obtain information about the topographic structure of the individual frequencies, the CSM was calculated between all pairs of coherence pairs for each frequency. In order to obtain information about the frequency structure of individual coherence pairs, the CSM was calculated between all pairs of frequency bins for each coherence pair. In addition, multivariate CSM was calculated over the entire frequency range for subsets of coherence pairs.

Bivariate or multivariate CSM characterizes the covariance structure of single data sets, but it cannot be used to compare different sets using their joint covariance structure. In order to compare the topographical structure of different frequencies, a paired Hotelling's T^2 statistic was calculated between all pairs of frequency bins for selected subsets of coherence pairs. In order to compare different subsets of coherence pairs, a paired Hotelling's T^2

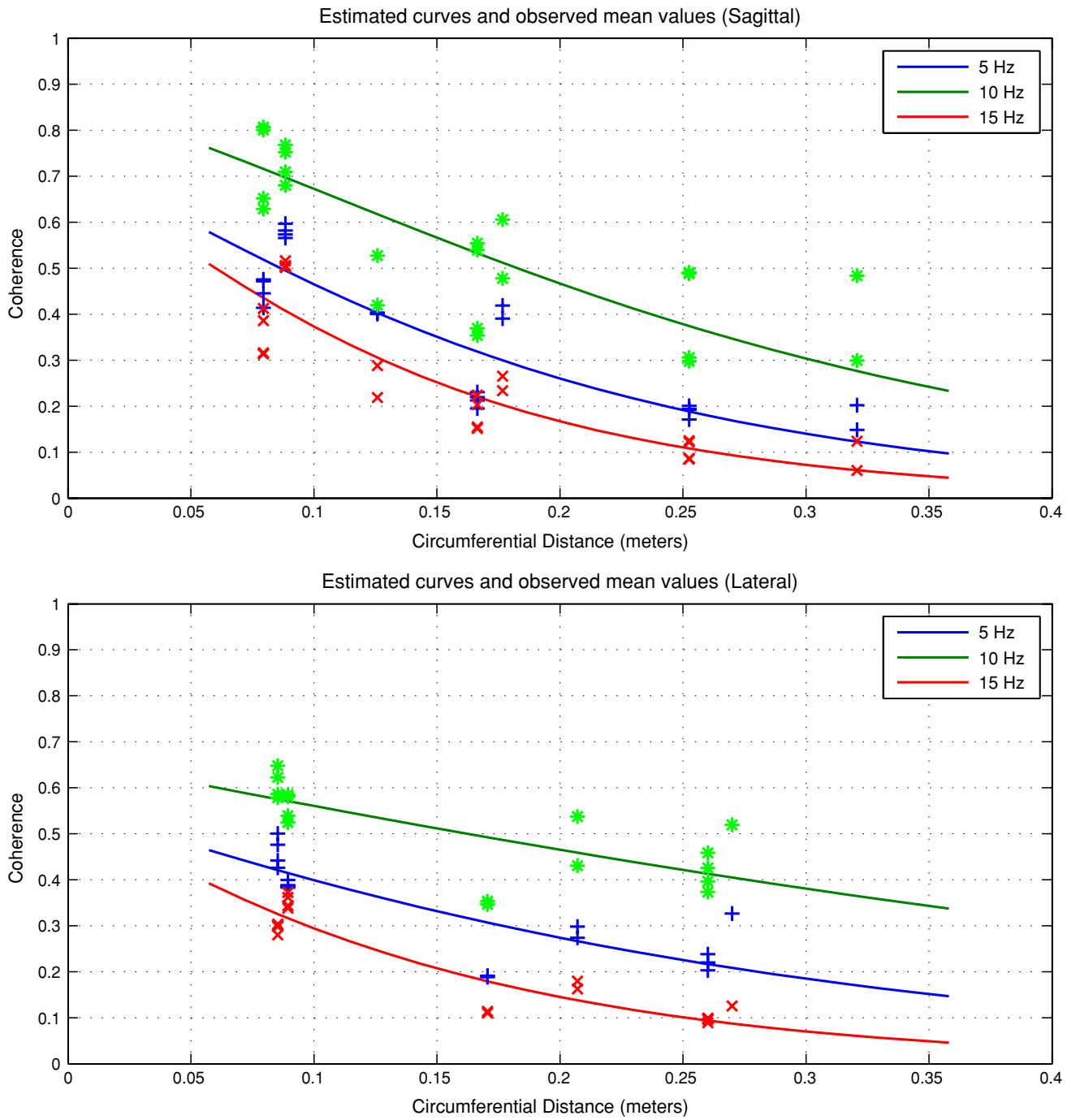

Fig. 2 Fit of $\gamma_{est}(R, f) = e^{-(a(f)+b(f)R)}$ to observed data. *Upper panel* sagittal pairs. *Lower panel* lateral pairs

statistic was calculated between comparable coherence pairs across subsets for each frequency bin.

Results

Distance modeling

Our interpretation of the coherence spectra is based on the following premise: a model for coherent activity generated by the dispersion of patterns of neural activity implies a decrease in coherence with distance (following Robinson 2003); the departures (residuals) from the model [the $\delta_{ij}(f)$ in "Aggregative measures and distance modeling"] in the aggregative measures are indicators of non-dispersive factors. By analyzing the departures from the model, the effects of the mean level of coherence at each frequency bin and of distance are removed, and the relative differences between coherence pairs are much more apparent.

This clarifies the frequency-specific differences in topographic structure. In order to be conservative, we tend to interpret only positive residuals as indicators of non-dispersive factors, such as additional sources of coherent activity or anatomical anisotropies. Negative residuals are considered to be simply the result of the fact that the total magnitude of the residuals is minimized, and have no neurophysiological or neuroanatomical significance.

The values for $a(f)$ and $b(f)$, obtained using the method in "Aggregative measures and distance modeling", were used to calculate isocoherence lines as a function of distance and frequency by $\gamma_{\text{est}}(R, f) = e^{-(a(f)+b(f)R)}$. The shape of the isocoherence lines so calculated is remarkably similar to that found in Robinson (2003, fig. 2, p. 167), giving plausibility to our use of the Robinson's theory (see Fig. 1). Further plausibility is given by the fact that all coherence spectra have generally the same shape, as shown in Fig. 3. We note that since they do not have exactly the same shape, not all coherence values at the same distance and frequency are equal. The fit of coherence as function of distance and frequency in the model is shown in Fig. 2 along with the mean values for selected frequencies. Lateral pairs show little divergence from the model. The divergence for the sagittal pairs is largest at the most distant interhemispheric pairs, which can be explained by their symmetrical character (see "Coherence in sagittal pairs") (since the model is intended for heuristic purposes, the failure of the curves to approach 1 when the distance approaches 0 is not considered an impediment to the use of the model).

Mean and peak values

Coherence at any given frequency decreases with distance, although not monotonically. Coherence peaks at about 10 Hz, and by 13 Hz falls to a level less than that of any lower frequency. It maintains relative constancy until about 20 Hz and then falls gradually with rising frequency. This pattern is characteristic of all coherence pairs, but the relative strength of coherence in different frequency bands across the complete spectrum varies considerably among natural groups of coherence pairs (as indicated in "Data selection"). Mean peak frequencies for coherence pairs lie between 7.5 and 11 Hz in the alpha band. Pairwise differences between peak values of coherence and frequency at peak value between all lateral pairs and all sagittal pairs were tested by paired t tests. Using a full Bonferroni correction, more differences in peak values of coherence between coherence pairs are statistically significant, 42%, than differences in frequency at peak value, 15%. The peak frequency differences which are significant are between anterior pairs not involving temporal electrodes, which have lower frequencies, and posterior pairs, which have higher frequencies, similar to those observed by Feshchenko et al. (2001). Individuals are clearly differentiated by overall strength of coherence values: a principal component analysis of peak values shows that the first component accounts for 58% of the variance of the sagittal peak values and 55% of the variance of the lateral peak values.

Frequency band structure

A non-topographic indication of similarity between individual frequency bins is given by the mean (across all coherence pairs) cross-frequency CSM, shown with the mean for each frequency separation removed (see Fig. 4) (means across subsets of coherence pairs show similar patterns). This is a measure based solely upon comparisons within single coherence pairs. We can reject non-banded models of frequency structure by demonstrating serial autocorrelation in the diagonals of the frequency structure matrices under the assumptions that the CSM for all pairs of frequencies having the same separation are either constant or have an AR(1) structure (local autocorrelation). The Durbin–Watson test (Durbin and Watson 1950, 1951) was used both on the mean-removed values and on the residuals after AR(1) modeling using the Burg method (Marple 1987). All coherence pairs showed serial autocorrelation in the residuals. As a check, permutation tests show that there is no serial autocorrelation in the permuted data. Similarity of banding between different coherence pairs was assessed by calculating the correlation coefficients between all coherence pairs of the diagonals of the mean removed frequency structure matrices with frequency separation 2 Hz, the separation with the greatest amount of serial autocorrelation. All correlation coefficients were greater than 0.2 and fewer than 14% were less than 0.5. [The correlation coefficients less than 0.3 were not anomalous, but consistent with other measures of similarity.]

The pattern of theta and beta CSM values can be explained by the existence of independent sources of coherent activity in each band. The pattern of low similarity between adjacent frequencies in the alpha band is the result of the fact that the peak frequencies occur in the alpha range and show considerable spread across frequencies in any pair and that the CSM is sensitive to the pattern of signs of the differences in values between different frequencies. The frequency variation of peaks may also be an indication of multiple sources of coherent alpha activity.

A topographic indication of similarity between individual frequency bins is provided by the paired T^2 statistic for the comparison of frequency bins calculated for subsets of the laterally and of the sagittally oriented coherence pairs (see Fig. 5 for sagittal values). As in the CSM, there are distinct theta, alpha, and beta frequency bands. Banding was similar in all subsets. Since the T^2 statistic, unlike the CSM, is not sensitive to the positions of peaks in the data,

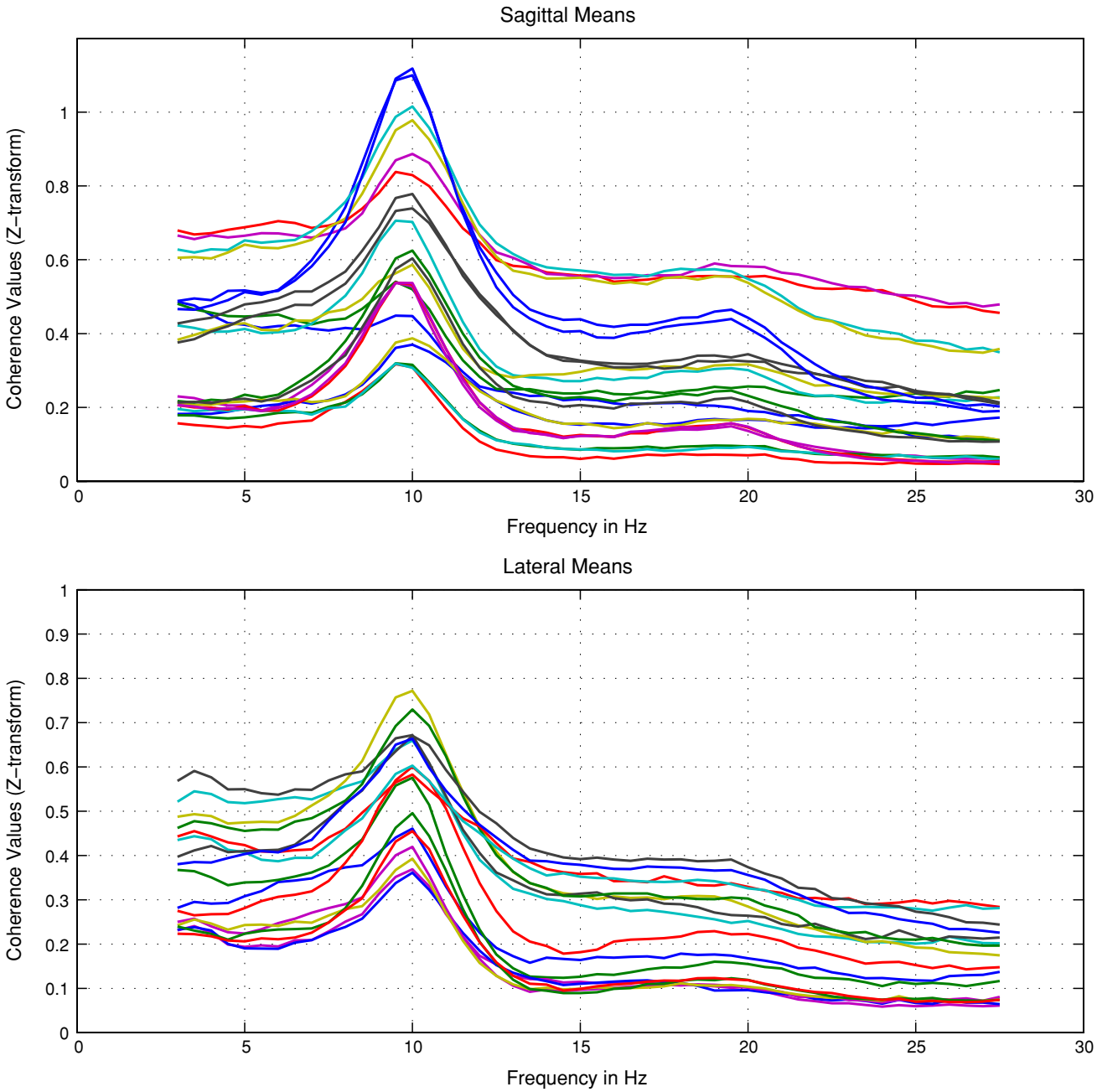

Fig. 3 Means of all coherence pairs included in the study. Note the general similarity in shape across all pairs, although relative values at different frequencies may be quite different

there is region of similarity in the alpha band corresponding to those in theta and beta.

Topographic structure

The connections which are significant at all frequencies are primarily parallel to or perpendicular to the anterior–posterior axis, as determined by the use of a minimum mean value across all frequencies in selecting the coherence pairs to include in the study. There were relatively few diagonally oriented pairs selected, none of which are long-distance. As stated in "Data selection", coherence pairs have natural groupings by locational characteristics: anterior or posterior, left or right, central or peripheral, containing a midline channel or not; and by relational characteristics: symmetric or asymmetric, adjacent or distant, and interhemispheric or intrahemispheric; and their combinations. We report on frequency-specific value related differences in all these characteristics. These differences indicate neuroanatomical features significant in coherent EEG activity. In addition to

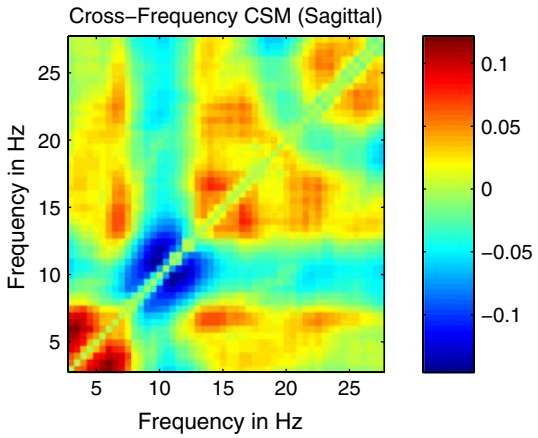

Fig. 4 Mean cross-frequency CSM for sagittal pairs. The mean for each frequency separation has been removed (mean removed $a_{i,j} = a_{i,j} - \frac{1}{N-k}\sum_{m=1}^{N-k} a_{m,m+k}$, where $k = |i - j|$.) Higher values (*red areas*) represent greater similarity. Low values (*blue areas*) in the alpha region reflect variation in the location of peaks in the coherence spectra. Lateral pairs are similar. This is a non-topographical measure of similarity

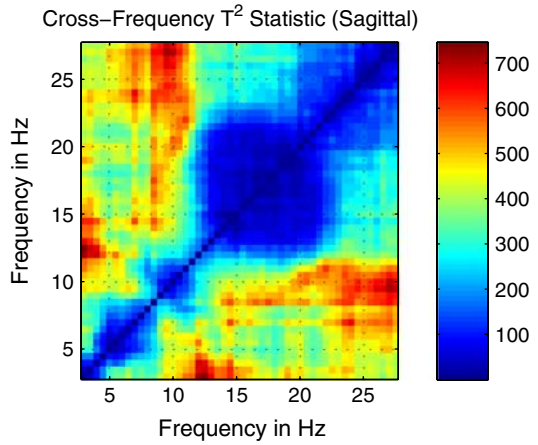

Fig. 5 Cross-frequency paired T^2 statistics for sagittal coherence pairs. Lower values (*blue areas*) represent greater similarity. Lateral pairs are similar. This is a topographical measure of similarity

this value related structure, the bivariate (pairwise) and multivariate covariance relations between coherence pairs determine an additional topographic structure. We report on the bivariate relations between corresponding anterior and posterior pairs, and corresponding central and peripheral pairs. We applied multidimensional scaling (MDS) to the bivariate CSM values to enable the visualization of the similarity relations between coherence pairs. These relations indicate related and unrelated complexes of coherent EEG activity. The axes determined by MDS applied to the bivariate measures between all pairs generally coincide with two locational distinctions, anterior/posterior and the presence or absence of a midline channel.

Examination of the residuals after distance modeling shows that natural groupings of coherence pairs (by location and distance) exhibit similar patterns which have frequency-specific differences. A detailed account of these results follows, which will describe the locational and relational structure of coherence, augmented by consideration of the frequency-specific grouping of the pairs into systems of connectivity by CSM.

Coherence in sagittal pairs

Frequency band separations are apparent upon examination of the residuals after distance modeling of the 22 sagittal interhemispheric coherence pairs (see Figs. 6, 8, 9), and of pairwise CSM between related pairs (see Fig. 7). The theta frequency band showed the most complex topographic structure. Coherent activity involving local (adjacent) midline pairs was found to be distinct from activity involving temporal pairs, which themselves exhibited a strong anterior/posterior differentiation. In contrast, alpha activity was marked by a posterior focus which extended into anterior regions, except for midline pairs which are not affected. Beta coherence was more localized (lower mean CSM) than either theta or alpha, particularly above 22 Hz. We examine each frequency band in turn, characterizing all coherence pairs in the band. All discussion of mean values will refer to the residuals which remain after the distance modeling. Differences in the residual plots greater than 0.1 are significant using paired t tests with full Bonferroni correction over the entire frequency range. Differences in the pairwise CSM greater than 0.05 are significant using paired $t$tests with full Bonferroni correction over the entire frequency range. [These statistical values were obtained by bootstrapping using 10,000 resamplings.]

Theta coherence generation has three distinct components. One component is midline, probably generated by local connections, and is stronger in the anterior than posterior region. There are two components involving peripheral sites, one anterior, and a stronger posterior one. The posterior component has a symmetry effect, i.e., the residuals for the symmetrical pairs are considerably larger than those at the asymmetrical pairs involving the same electrodes. In addition, anterior theta coherence becomes more uniform across pairs with increasing frequency by CSM, while posterior pairs separate into two distinct groups with increasing frequency.

The midline local contribution to theta is apparent in the examination of the sagittal asymmetric coherence pairs (Figs. 8, 9), in which the adjacent midline pairs are consistently larger than the adjacent temporal pairs. Since all adjacent pairs are the same distance apart, the difference between temporal and midline pairs can only be the effect of location. We also note that the midline difference from the non-midline is about twice as large anteriorly than posteriorly in the adjacent pairs. In contrast, the

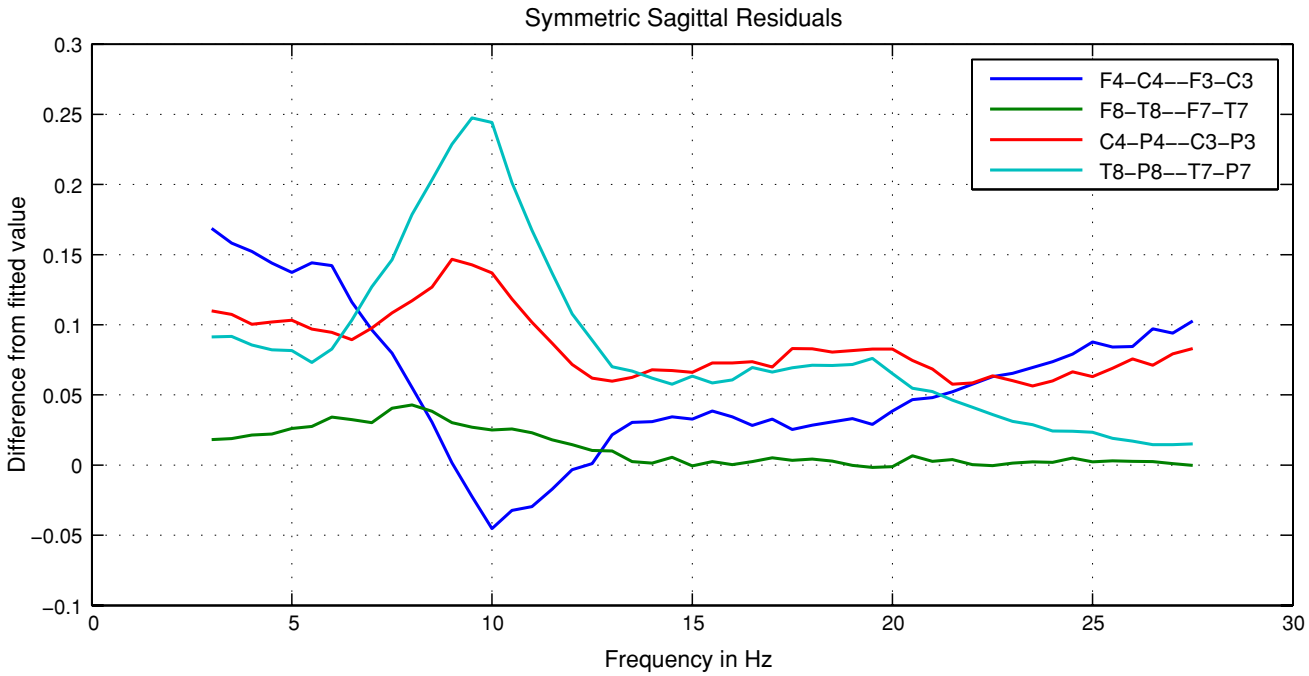

Fig. 6 Residuals after exponential distance modeling for symmetric sagittal pairs

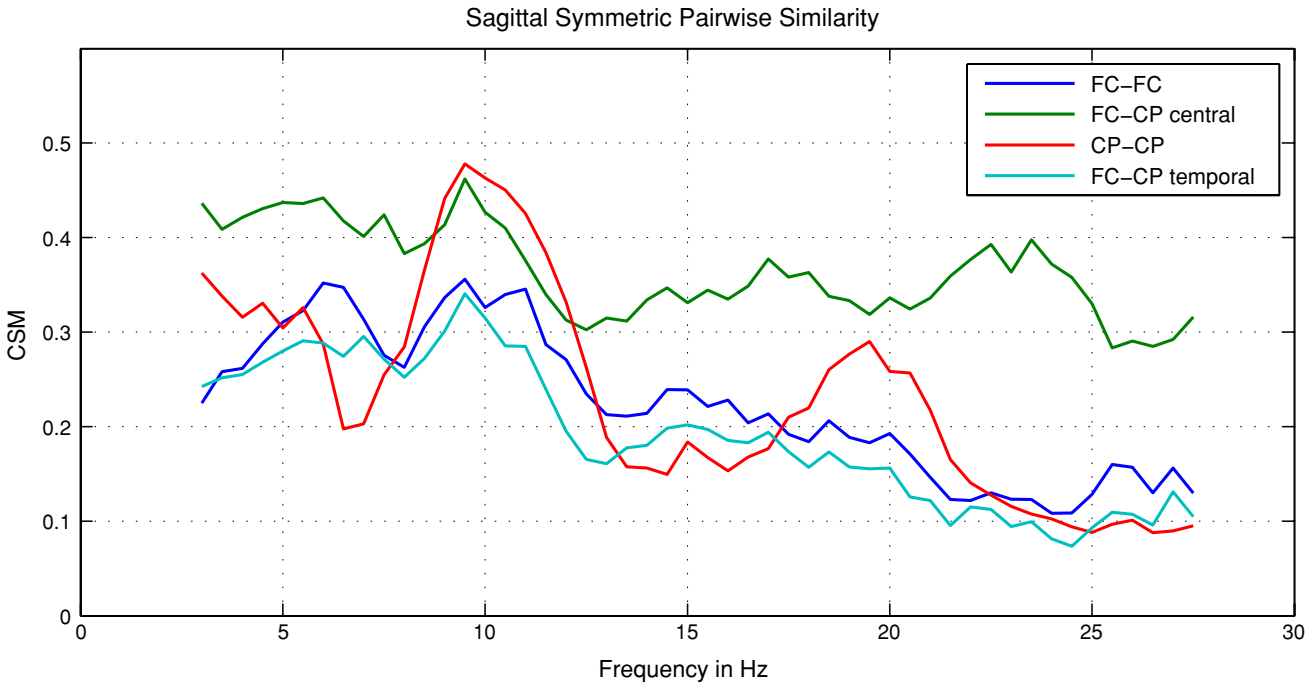

Fig. 7 Pairwise correlational similarity (CSM) for symmetric sagittal pairs. FC-FC is F4-C4–F3-C3 with F8-T8–F7-T7; FC-CP central is F4-C4–F3-C3 with C4-P4–C3-P3; CP-CP is C4-P4–C3-P3 with T8-P8–T7-P7; FC-CP temporal is F8-T8–F7-T7 with T8-P8–T7-P7

non-adjacent pairs not containing a midline electrode are consistently larger than those which do. This implies that the midline effect is purely local. The presence of specifically symmetric posterior temporal activity is evidenced in the symmetrically placed pairs (Fig. 6); the temporal symmetrical pair T8-P8–T7-P7 is consistently larger than either T8-P8–C3-P3 or T7-P7–C4-P4; this is not the case for the corresponding anterior pairs. Consideration of theta CSM values shows a division occurring about 6 Hz between low and high theta bands. Symmetrical internal anterior and posterior pairs have consistently high similarity, while symmetrical peripheral anterior and posterior

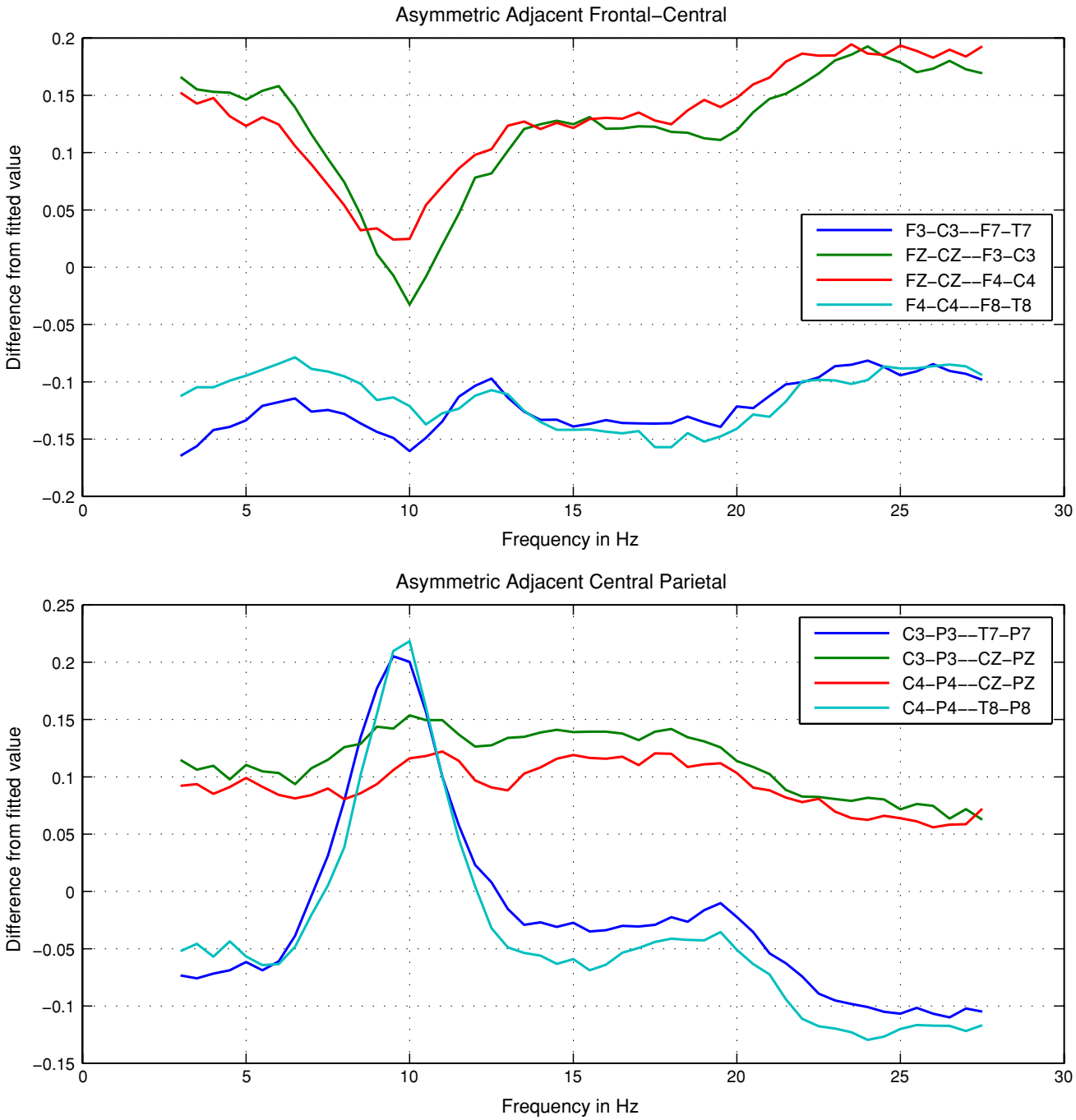

Fig. 8 Residuals after exponential distance modeling for adjacent asymmetric sagittal pairs. Fronto-central pairs are above centro-parietal pairs. Pairs including a midline electrode are *red* and *green*; pairs not including a midline electrode are *blue* and *cyan*. The locations in each of the adjacent pairs are the same distance apart

pairs have low similarity. Anterior symmetrical pairs have increasing similarity with higher frequency, while posterior symmetrical pairs have decreasing similarity with higher frequency (Fig. 7).

The structure of alpha coherence is different from theta; it has a strong posterior focus and a large degree of correlational similarity across the posterior zone as can be seen in Fig. 13. There is is a considerable difference in magnitude in the 8–13 Hz range between the anterior and posterior regions. In examining the posterior coherence pairs, all show a significant increase in residual value except those including midline electrodes. The increase was greatest in adjacent non-midline (intrahemispheric) coherence pairs, and was also accompanied by a considerable increase of the CSM between those pairs. There is also a considerable increase in the temporal symmetric

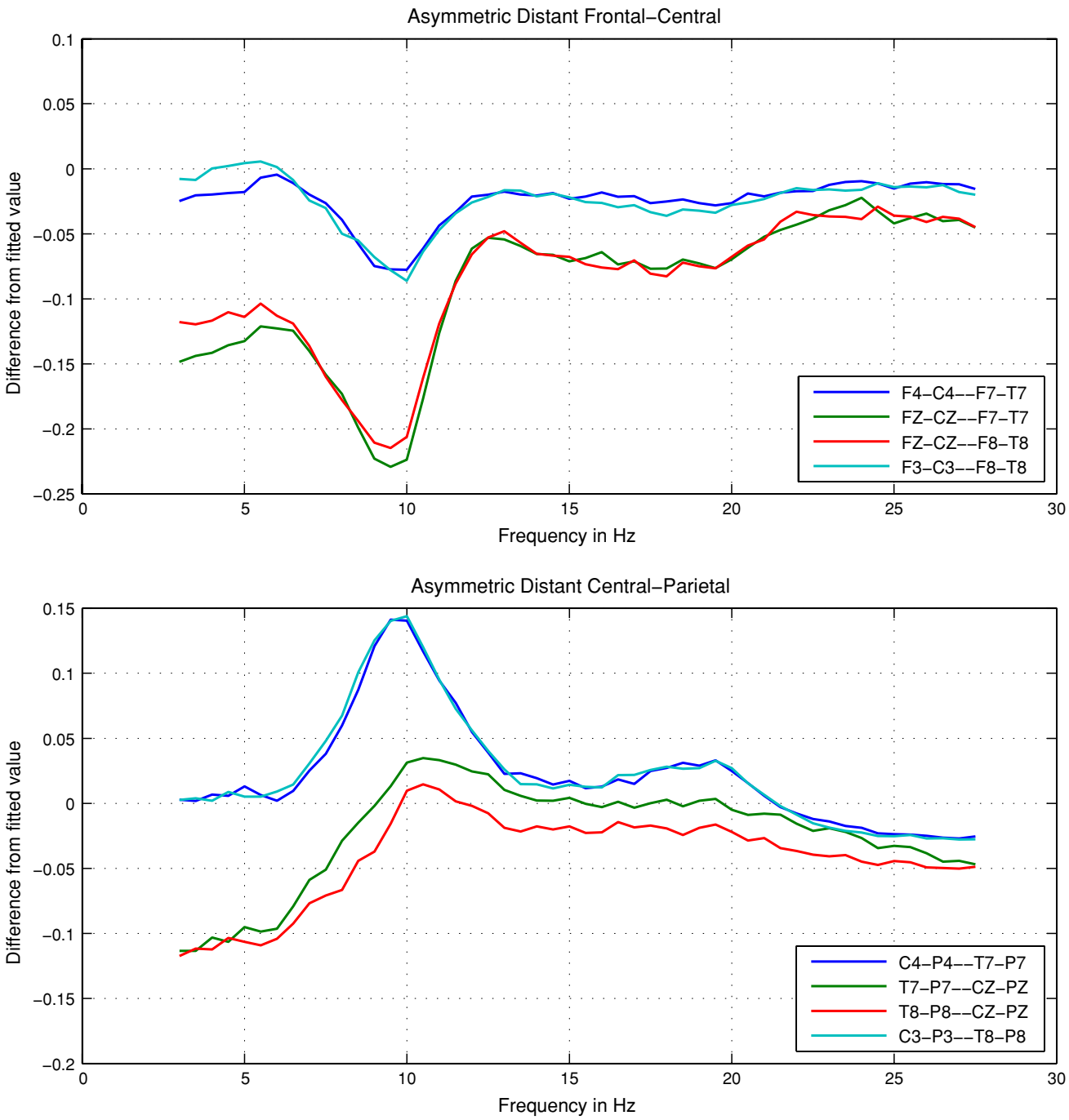

Fig. 9 Residuals after exponential distance modeling for distant asymmetric sagittal pairs. Fronto-central pairs are above centro-parietal pairs. Pairs including a midline electrode are *red* and *green*; pairs not including a midline electrode are *blue* and *cyan*. The locations including a midline electrode are closer than those not including a midline electrode

coherence pair, suggesting the continuation of temporal symmetric effect found in the theta band. Anterior pairs displayed a pattern different from that of the posterior pairs. Intrahemispheric values did not surpass midline values and temporal symmetric values were only marginally larger than internal symmetric values. Particulary striking was the decrease in CSM between interhemispheric and intrahemispheric pairs in low alpha, not seen in posterior pairs (see Fig. 10). These findings are consistent with studies showing multiple sources of alpha activity, as discussed in "Comparison to EEG and MEG studies".

Coherent beta activity has a slight midline focus, as the residuals of the adjacent asymmetric midline coherence pairs are all positive. In contrast, the residuals of the non-adjacent asymmetric coherence pairs are primarily negative. This suggests that beta has a local midline plus symmetrical

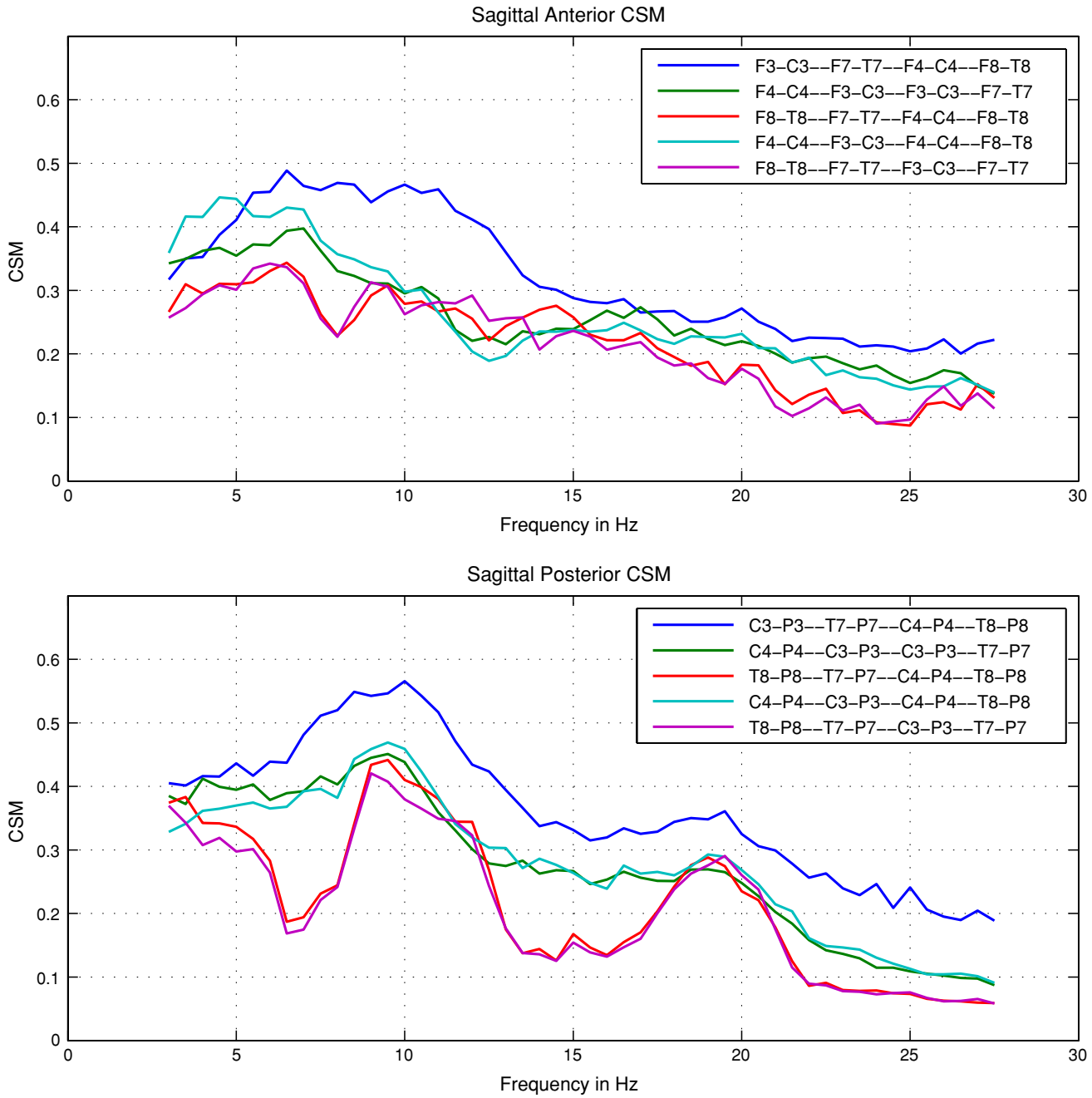

Fig. 10 Sagittal anterior and posterior homologous pairwise similarity measures. *Blue lines* are intrahemispheric pair CSMs. *Green* and *cyan lines* are central interhemispheric with intrahemispheric CSMs. *Red* and *magenta lines* are temporal interhemispheric with intrahemispheric CSMs

pattern, making in more like theta and less like alpha. High beta (22–28 Hz) may be distinguished from low beta (14–19 Hz) by greater differences in values for homologous anterior and posterior coherence pairs (Figs. 8, 9).

Coherence in lateral pairs

We note that the variance of the residuals of the lateral coherence pairs is considerably smaller for all frequencies than the variance of the residuals of the sagittal coherence pairs, even though the lateral coherence pairs include interhemispheric, intrahemispheric, and diagonally oriented pairs (see Figs. 11, 12).

Lateral intrahemispheric theta is characterized by a difference between anterior elements, which show a relative decline from low to high theta, in contrast to a relative increase for posterior elements. Interhemispheric theta is higher centrally than either anteriorly or

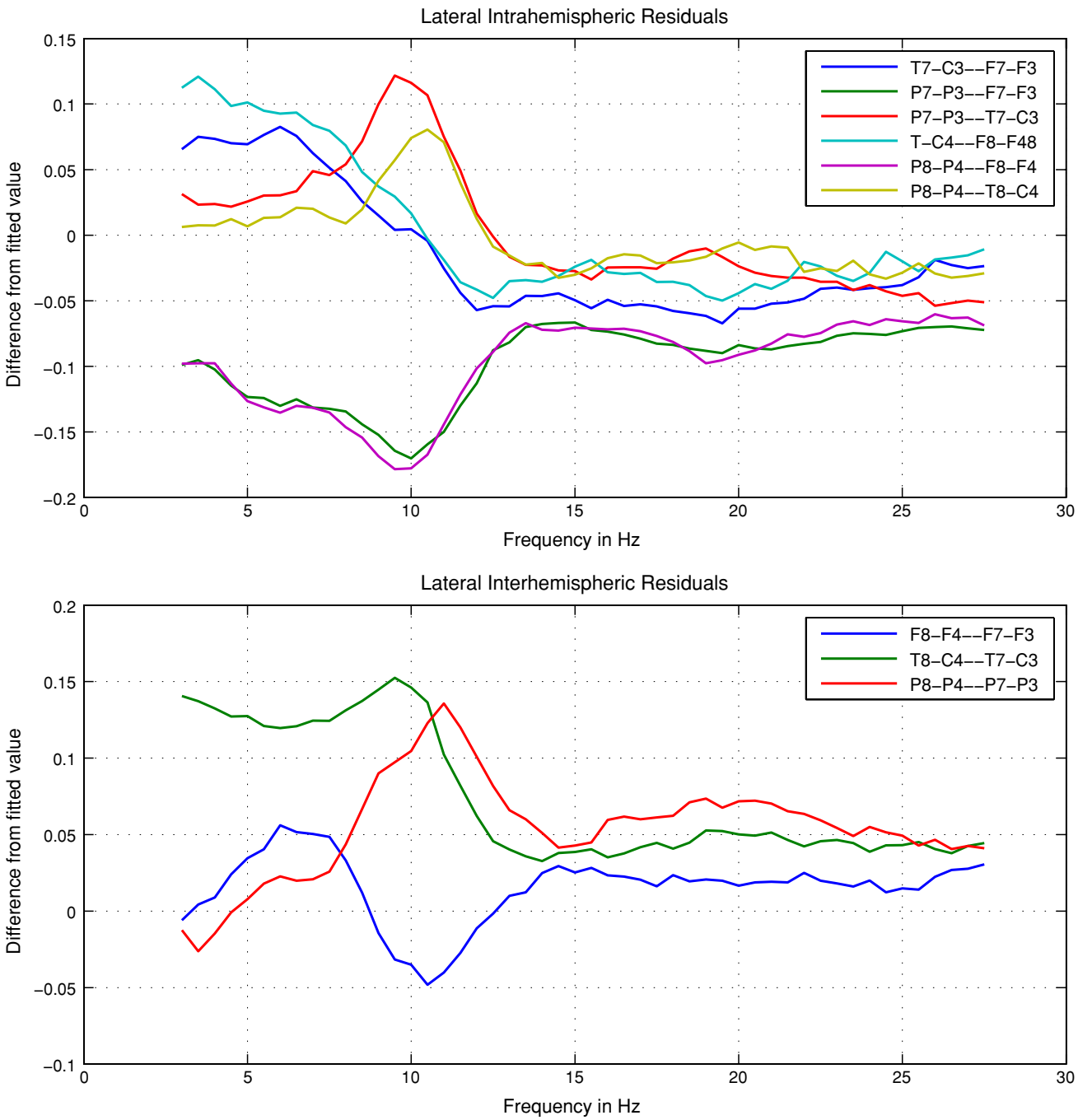

Fig. 11 Residuals after exponential distance modeling for lateral intrahemispheric and interhemispheric pairs

posteriorly; the increase with frequency in the anterior and posterior coherence pairs does not correspond to anything in the sagittal coherence pairs. The low values for midline intrahemispheric theta suggest that the local connections evidenced in midline sagittal pairs are primarily between hemispheres, rather than along the midline itself.

In the alpha band the posterior focus found in sagittal pairs is also found in lateral pairs. The increases in both interhemispheric and intrahemispheric coherence pairs is less than that found in the sagittal pairs. As in the sagittal pairs, there is no midline effect.

In the beta band the elevation of the intrahemispheric midline pairs, although slight, suggests that coherent activity may be along the midline, unlike the situation in theta. The relative change from low to high beta found in the sagittal coherence pairs was also found in the lateral pairs, although not to as great a degree.

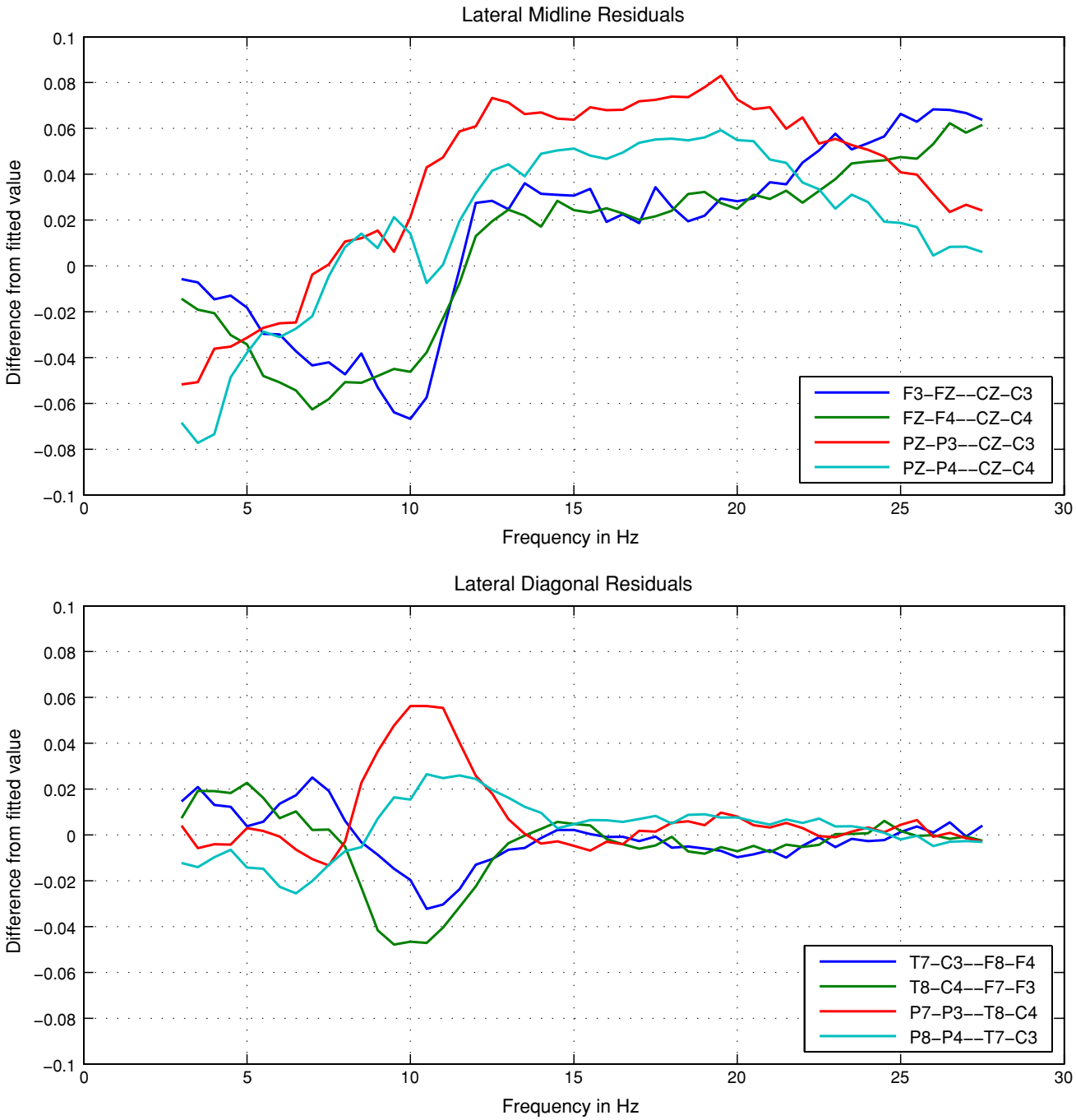

Fig. 12 Residuals after exponential distance modeling for lateral midline and diagonal pairs. Note that the scale of intrahemispheric and interhemispheric lateral pairs is considerably larger than that of the midline and diagonal pairs

Topographic structure: correlational similarity

Systems of coherent EEG activity are indicated by correlational similarity between different coherence pairs at the same frequency. We illustrate the frequency-specific characteristics by plots in which the coherence pairs are represented at coordinates obtained from MDS via the Isomap algorithm (Tenenbaum et al. 2000) applied to the pairwise similarity measures (CSM) between different coherence pairs at each frequency. MDS provides an interpretable map of the relations among all the items whose similarity has been determined. It places two pairs near each other based on their relation to all other pairs, not simply because they are similar to each other. The Isomap algorithm is a non-linear dimensionality reduction method which uses local distance relations, here provided by the

pairwise similarity measures, to produce a global two-dimensional surface on which to place the points whose distances are provided. In addition, in our plots the pairs which are very similar ($CSM > 0.45$) are connected with lines, and the actual coherence values are represented by the size of the circles at the locations of the pairs. It should be emphasized that the fact that coordinate axes in these plots represent significant topographical relations, e.g., anterior–posterior for the *Y*-axes for the sagittal pairs, is not dependent upon the actual locations of the coherence pairs on the scalp but it is a consequence of correlational similarities alone. That is, correlational relations correspond to locational characteristics in general, but more strongly in the theta and alpha bands than in beta. In contrast, high levels of pairwise similarity are frequency specific. We have separated sagittal and lateral pairs because MDS applied to the combined data always shows a clear separation between sagittal and lateral pairs.

We have selected four frequencies for display, each of which displays a different pattern of connectivity, each consistent with the pattern shown by the analysis of coherence values. In the sagittal pairs, theta band coherence has a complex topographic structure in which there are patterns of differentiation between anterior and posterior peripheral locations but similarity between anterior and posterior midline locations. In contrast, alpha band coherence has much stronger similarities posteriorly than anteriorly. Beta band coherence has a considerable lower levels of correlational similarity between pairs than theta or alpha. In all sagittal cases, the *Y*-axis represents an anterior–posterior axis and the *X*-axis in theta and alpha represents to a large extent a midline-peripheral axis. The spatial patterns are more difficult to characterize in the lateral pairs, since they include both interhemispheric and intrahemispheric pairs with varying orientations. Generally, the *X*-axis represents an interhemispheric–intrahemispheric axis, while no consistent interpretation can be attached to the *Y*-axis. These plots suggest that there are shifting complexes of related coherence pairs, which seem to be more clearly delineated in the sagittal pairs. Examination of pairwise CSM graphs (four comparisons shown in Fig. 7) reveals patterns of both consistent and intermittent similarity across frequencies, depending on the location.

Summary: frequency-specific topographic structure

The framework of axial connectivity is established by the selection of the coherence pairs meeting a minimum value criterion, fewer than 30% of the number of possible pairings. Topographic structure, based both on similarities of the mean values of the residuals of modeled coherence spectra, and on correlational similarity, is frequency specific. In order to recapitulate, theta band coherence has a complex topographic structure in which there are patterns of differentiation between anterior and posterior peripheral locations but similarity between anterior and posterior midline locations. In contrast, alpha band coherence has a clear posterior focus with a much larger difference in values between anterior and posterior than in the theta band. Beta band coherence is highly localized with little global structure. There is little left–right differentiation in any frequency band. Frequency structure is similar whether based on cross-frequency similarity at individual coherence pairs or cross-frequency topographical similarity. The structure is one of banding into theta, alpha, and beta bands, with subdivisions in the theta and beta bands. The divisions between frequency bands are generally similar across all natural topographic groups of coherence pairs; they are not greatly locationally specific. Although differentiations between locations and frequencies are clear, the characterization of separate factors of coherent EEG activity, whether anatomical or physiological, must remain tentative at this point.

Discussion

Our results establishing the frequency-specific topographic structure of EEG coherence lead us to the following conclusions:

1. The similarity across coherence pairs of frequency banding determined by relations between individual coherence pairs, shown by the relative values of the coherence spectra in individual coherence pairs and the CSM between individual coherence pairs, implies that there are different frequency-specific neurophysiological sources of coherent activity whose action is independent of location.
2. The similarity of banding determined by topographic relations to the banding within coherence pairs, as shown by Hotelling's T^2 statistic and the CSM between coherence pairs (compare Figs. 4 and 5), implies that locationally different neuroanatomical features have different effects at different frequencies. That is, if locationally different neuroanatomical features had the same effects for different frequencies, then there would be no topographic banding effects, i.e., topographic relations would be the same regardless of frequency.
3. The variability of cross-location CSM across frequencies (Fig. 7) implies that complexes of highly similar locations are frequency specific, as shown in Figs. 13, 14. In addition, examination of pairwise CSM plots show repetition of complexes possibly exhibiting harmonic relations, as suggested by Robinson (2003, p. 167).
4. The roughly similar shape of coherence spectra at all coherence pairs suggests that even with the

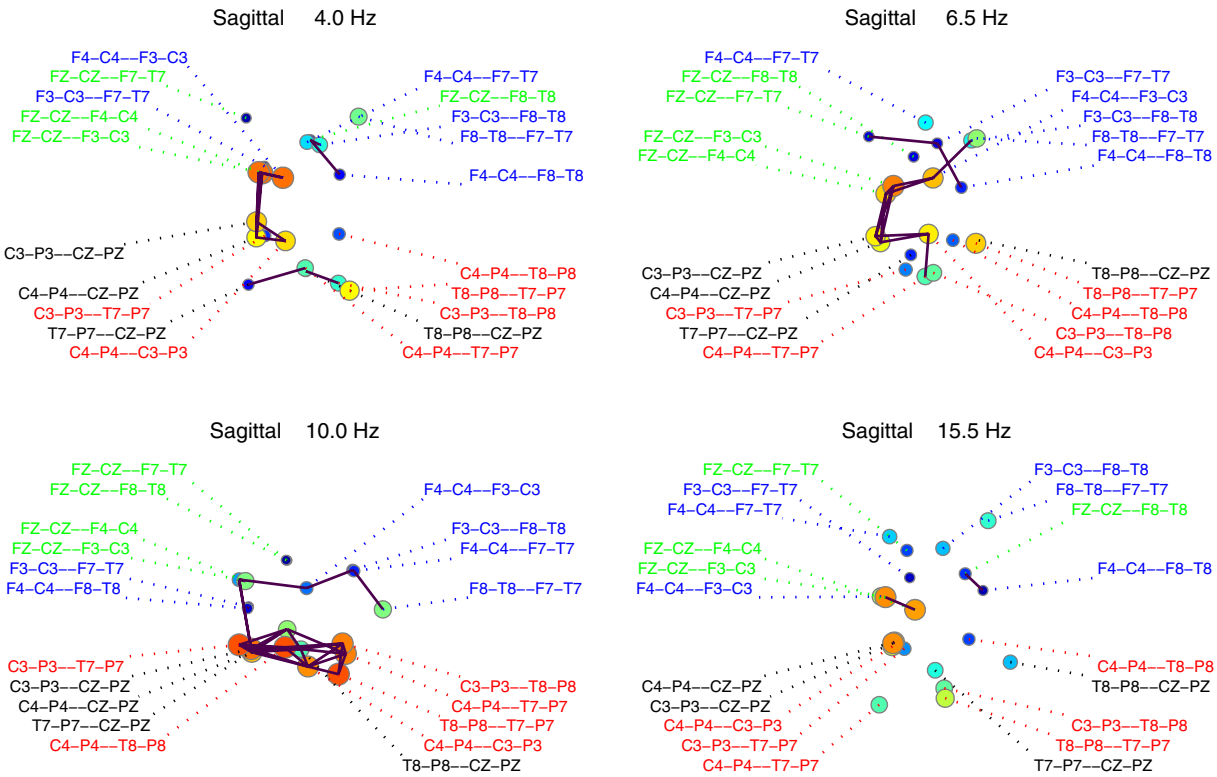

Fig. 13 Sagittal interpair relations for selected frequencies. The position of coherence pairs is derived from multidimensional scaling of the isomap transformation of the pairwise CSM. *Lines* indicate significant similarities between pairs ($CSM > 0.45$). Size and *color* of circular markers indicate size of residual after modeling. Coherence pair names are color coded: *blue* fronto-central non-midline, *red* centro-parietal non-midline, *green* fronto-central midline, *black* centro-parietal midline (coordinates were rotated to make individual frequencies comparable). Note that the *X*-axis represents an temporal-midline axis for the theta and alpha bands, while the *Y*-axis represents an anterior–posterior axis for all frequencies

localization given by the use of bipolar derivations, multiple sources of coherent activity are being recorded at each scalp location.

The existence of RSN of brain activity shown by fMRI studies raises the question of the character of the neural processes which coordinate the activity of those dispersed systems. If scalp-recorded EEG has topographic patterns similar to those of RSN, then we suggest that the neural processes which coordinate the activity of dispersed networks may be related to those producing EEG. The frequency-specific topography of resting state EEG coherence suggests that the neural activity responsible for different RSN may have distinct frequency spectra. The most comprehensive fMRI studies of the topographic structures of resting-state neural activity are those of Salvador et al. (2005) and of Mantini et al. (2007). We shall offer an interpretation of these structures in light of the results obtained here. Before proceeding to that interpretation, we briefly remark on a number of studies which discuss topographic patterns of neural activity in the resting state using a variety of methods. In addition to EEG studies, these methods include magnetoencephalography (MEG) and fMRI with and without concurrent EEG recording. Although MEG studies are capable of frequency-specific results, it is not possible for fMRI studies to determine the frequency of the activity whose location is found. Concurrent recording of EEG with fMRI enables some elements of the correlation between EEG measures and the hemodynamic quantities measured by fMRI to be determined. Because of the different limitations of both EEG and fMRI recording techniques, the topographical similarities found between our results and those obtained by fMRI studies are suggestive rather than probative.

Sources of coherent activity

Our study considers only coherence measured in the resting state; the relation of coherence measured in task-related conditions to resting-state coherence is too large a topic to be discussed here. Our study does not attempt to determine the neurophysiological sources of coherent EEG activity, although our interpretation of the data can hardly avoid addressing this issue. Coherent activity has been explained

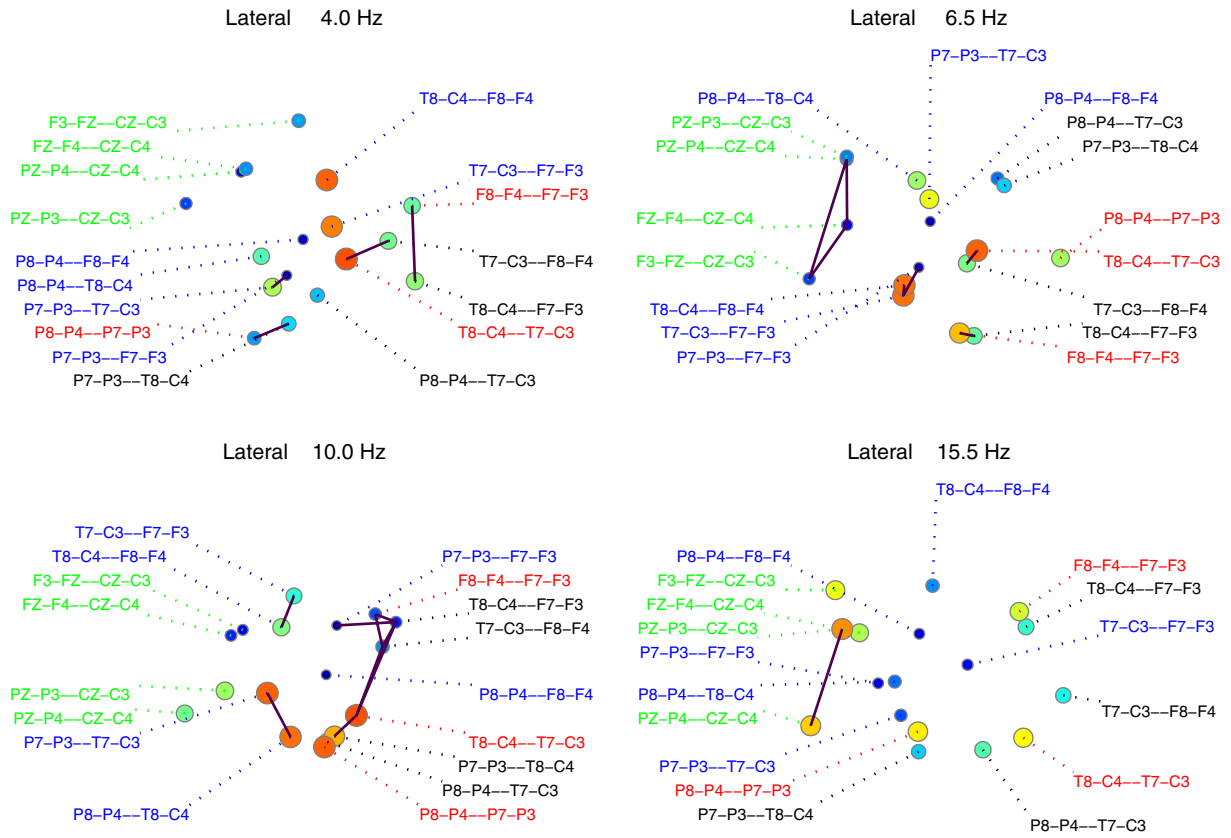

Fig. 14 Lateral interpair relations for selected frequencies. The position of coherence pairs is derived from multidimensional scaling of the isomap transformation of the pairwise CSM. *Lines* indicate significant similarities between pairs (*CSM* > 0.45). Size and *color* of circular markers indicate size of residual after modeling. Coherence pair names are color coded: *blue* peripheral intrahemispheric, *green* midline intrahemispheric, *red* symmetrical interhemispheric, *black* diagonal interhemispheric (coordinates were rotated to make individual frequencies comparable). Note that although the *X*-axis represents to some degree an intrahemispheric-interhemispheric axis, no consistent interpretation can be attached to the *Y*-axis

as the product of thalamocortical circuits and also as the product of corticocortical connections. [For illustrations of different models, see Hughes and John (1999; fig. 1) and Thatcher et al. (1986, fig. 9).] In addition, there may be effects of global spatial fields (Srinivasan et al. 2006; Nunez and Srinivasan 2006). It is likely that the explanation is different for different frequency bands. For example, some evidence indicates the salience of thalamocortical circuits in the explanation of theta activity (Sarnthein et al. 2005; Sarnthein and Jeanmonod 2007) and alpha activity (Schreckenberger et al. 2004; Feige et al. 2005; Goldman et al. 2002; Hughes and Crunelli 2005), although there are opposing views for alpha (Srinivasan 1999; Karameh et al. 2006; Cantero et al. 2002). It is also possible that the correlational separation between lateral and sagittal pairs (see "Topographic structure: correlational similarity") indicates the effect of distinct neuroanatomical factors at the same frequency. [See Hagmann et al. (2008; fig. 3) for an illustration of distinct laterally and sagitally oriented pathways.]

Comparison to EEG and MEG studies

Frequency-specific patterns of connectivity are also found in EEG studies of coherence in children by Murias et al. (2007a,b), although the results are not directly comparable to ours because of different methodologies and subject characteristics. Those studies were focused on finding EEG characteristics with which to distinguish two groups, not to establish general characteristics of a control group. Breakspear and Terry (2002) also provide an EEG study of relations between different areas of the brain, but their methodology and the sparsity of their topography makes a comparison unfruitful. The high degree of coherence in sagittally oriented temporal alpha is similar to that found by Cover et al. (2004) using MEG. Two studies of alpha band coherence are of direct relevance. Our results are broadly consistent with those of Srinivasan (1999), while some of our differences with Feshchenko et al. (2001) indicate a need to augment their model of alpha generation to provide a more satisfactory explanation of coherent activity.

One of the more significant papers on resting EEG coherence, both from the point of view of methodology and of results, is the study by Srinivasan (1999) of alpha band coherence. It uses coherence values from both potential and Laplacian derivations on observations of both children and adults, with an emphasis on long-distance coherence pairs. For adults, coherence values derived from potentials have a different structure than those derived from Laplacians. In values derived from potentials, intrahemispheric values are larger than interhemispheric values at comparable distances, and intrahemispheric values increase with distance as the distance between electrodes increases from 15 to 20 cm. Anterior interhemispheric values do not differ from posterior interhemispheric values. In values derived from Laplacians, posterior interhemispheric values are larger than intrahemispheric values which are larger than anterior interhemispheric values. There is no increase in coherence values with greater separation between electrodes. Our results more resemble those for Laplacians than those for potentials, in that posterior alpha values are greater than anterior alpha values for both sagittal and lateral derivations, that there is no increase with distance, and that the interhemispheric values are not too different from the intrahemispheric values when adjusted for distance. Mean values seem to be intermediate between the potential and Laplacian data. However, since we use a subset of the possible pairings (39 of 132), there can be no direct comparison of mean values. Srinivasan (1999) explains the difference between the potential and Laplacian data as "... the Laplacian also removed the contribution of the global spatial structure of the alpha rhythm that contributes to long-range coherence between anterior and posterior electrodes." (Srinivasan 1999, p. 1360) as a result of the spatial band-pass filtering of the Laplacian (Srinivasan et al. 1998; Srinivasan 1999). We note that Srinivasan et al. (2007) attributes some increase in coherence from potential derivations at longer distances to volume conduction effects, a phenomenon which does not occur for Laplacian derivations, so that the difference between the potential and Laplacian results may be partially the result of inflation of the potential values by volume conduction. Anterior–posterior differences found in the Laplacian are explained as the result of posterior callosal fiber systems (Srinivasan 1999, p. 1360). This difference is not found in the potential derivations because the volume conduction effects are large enough to obscure the anterior–posterior difference. We conclude from the similarities between the bipolar and Laplacian results that the bipolar derivation has some of the same spatial filtering properties as the Laplacian, so that while it eliminates some of the volume conduction effects, it may also underestimate some long distance coherence. This difference between the results of the use of bipolar derivations and potentials also explains why our results differ from those of Thatcher et al. (1986). Thatcher et al. (1986) advanced an explanation of coherent activity as the product of two distinct systems of corticocortical connections, one short-range and the other long range. One of the predictions was that long-distance coherence should be larger than that predicted from a model with exponential decrease of coherence with distance, as we have used. In lateral intrahemispheric data, which is the condition most similar to what Thatcher et al. (1986) consider, long distance coherence is lower than predicted by the distance model in all frequencies. This is consistent with the Laplacian results of Srinivasan (1999), while the results of Thatcher et al. (1986) are consistent with the potential results of Srinivasan (1999), showing volume conduction effects (Robinson 2003, p. 169).

Coherence results are a significant feature of the study of alpha band activity by Feshchenko et al. (2001). That study differentiated three distinct rhythms in the alpha range on the basis of topography, peak frequency and attenuation by activity. According to that study, in most subjects the anterior alpha band rhythm is an extension of the primary posterior alpha rhythm, but an anterior alpha band rhythm independent of the primary posterior alpha rhythm is present in a subset of the population. An additional posterior mu rhythm may also be present. Our results are not inconsistent with the presence of multiple rhythms with these characteristics. This is evidenced in our data of the presence of local maxima of CSM at 10 Hz between posterior and corresponding anterior coherence pairs, as well as a much greater increase of CSM between posterior coherence pairs as compared to anterior pairs. Another indication of anterior–posterior differentiation is the decline in CSM between anterior sagittal intrahemispheric pairs and anterior sagittal interhemispheric pairs in the alpha band (see Fig. 10). We are not reliably able to differentiate a posterior mu rhythm from a posterior alpha. The cross-correlation ("CCC") values obtained by Feshchenko et al. (2001) are comparable to coherence values obtained from potential derivations, and will be treated as such. The CCC values for intrahemispheric pairs are similar to the coherence values obtained by Srinivasan (1999) for potential derivations, and the difference from our results has the same explanation as that given in our discussion of Srinivasan (1999) above. However, there are significant differences between our results with regard to interhemispheric coherences that deserve a more detailed discussion.

Feshchenko et al. (2001) finds high interhemispheric coherences, no anterior–posterior differences in coherences, no correlation of the parameters of the model for alpha generation between hemispheres, thus no correlation of the coherence values with the parameters of the model for alpha generation, and concludes that the high coherence values are the result of correlated "broadband" input to the generators of alpha activity, not of any similarity between the alpha generators in the two hemispheres (Feshchenko et al. 2001,

pp. 337, 339). Activity in the 7 Hz (high theta) range is considered an appropriate measure of the broadband input. We find considerable anterior–posterior differences in coherences, considerable interhemispheric similarity, particularly posterior, using covariance measures, and lack of correlation between the coherences in the theta band and coherences in the alpha band. From this we conclude that alpha band coherence is relatively independent of activity in other bands, and that there is considerable similarity between the hemispheres. The difference in coherence values between our results and those of Feshchenko et al. (2001) is the effect of volume conduction on monopolar values used in that study, primarily the effect of midline activity where the difference between anterior and posterior is least. Other differences, particularly with regard to the cause of interhemispheric alpha band coherence and interhemispheric similarity are the result of somewhat different perspectives on data analysis.

The study by Feshchenko et al. (2001) is oriented toward determining parameters for individuals under a specific model of alpha generation, whereas our study makes use of Robinson's model applied to mean data as a heuristic to identify features of interest. The model used in Feshchenko et al. (2001) may be a satisfactory first approximation for single-site alpha activity, but an augmented model which incorporates the possibility of generators at multiple frequencies and interaction between sites would be more adequate to the task of explaining coherent activity and its variation across frequencies (Kaminski et al. 2001). In particular, Feshchenko et al. (2001) assume that scalp measured 7 Hz activity can be considered as an indicator of subcortical broadband input to cortical alpha generators. The presence of a distinct spatial covariance structure for coherent activity in the theta band, whose boundaries coincide with those of direct interfrequency covariance structures strongly suggests scalp measured theta activity cannot be regarded as a broadband noise process. In this circumstance, coherent alpha activity cannot be explained as the result of coherent input to alpha generators, thus leaving interaction between the generators as the remaining hypothesis. With regard to the independence of the generators in the hemispheres, we can only provide evidence regarding coherent activity, not the parameters of a specific model of alpha generation. Our results are that interhemispheric and intrahemispheric alpha band coherent activity in sagittally oriented pairs is the result of factors which are symmetrically similar between the hemispheres but exhibit a midline to temporal gradient within each hemisphere. This is shown by the fact that the CSM between the intrahemispheric pairs is always larger than the CSM between the interhemispheric pairs, which is larger than the CSM between an interhemispheric and an intrahemispheric pair which share a location. Similarly, in lateral intrahemispheric pairs, interhemispheric CSM is larger than intrahemispheric CSM in the alpha band. We regard our differences with Feshchenko et al. (2001) primarily as the result of different data modeling and analysis choices which lead to differences in interpretation but whose results could be encompassed by a more comprehensive model than either study provides.

Concurrent fMRI and EEG studies

There have been a number of studies in which EEG was recorded concurrently with fMRI in a resting state (Goldman et al. 2002; Laufs et al. 2003a, b; Feige et al. 2005; Moosmann et al. 2003) which focus primarily on the neural correlates of alpha activity and not particularly on connectivity patterns between the different neural regions. In Goldman's study, the alpha EEG activity in the occipital regions in which we found coherent alpha activity is negatively correlated with the MRI BOLD signal. Goldman suggests that alpha production is an aspect of reduced cortical activity (Goldman et al. 2002, p. 2490). Feige et al. (2005) also found that alpha activity in occipital regions we associate with coherent alpha activity is negatively correlated with the MRI BOLD signal. In contrast, Laufs et al. (2003a, b) found sites (not including occipital areas) at which the MRI BOLD signal was positively correlated with alpha activity. However, their later reanalysis of the data (Laufs et al. 2006) shows that there is a parietal–occipital negative correlation between BOLD and alpha power which occurs when other spectral measures indicate a possibly lower level of vigilance than when the negative correlation between BOLD and alpha power has a more frontal focus. An explanation of these phenomena is offered by Nunez and Silberstein: "Increases in neural firing rates may occur with reduced large-scale synchrony of current sources, and, as a result, smaller electric or magnetic scalp fields. By contrast, hemodynamic and metabolic measures are believed to increase with neural firing rates." (Nunez and Silberstein 2000, p. 79).

fMRI connectivity studies

There have been a number of fMRI studies investigating the functional connectivity of resting-state or default-mode activity. In experimental situations with alternations of task-related activity and "rest", some sites show increased activation in the resting state. Clearly, the brain activity measured in these studies is similar to that measured in studies of the resting EEG. It follows that the connectivity patterns found by fMRI studies may correspond to those found by the coherence measures detailed in studies of the resting EEG.

A number of studies show isolated results consistent with our own. One of the key structures identified by Greicius et al. (2003) associated with the default mode network was the posterior cingulate cortex. It had significant connection

with the both the left and right inferior parietal cortex. This association reproduces a pattern that is remarkably similar to that found in posterior theta coherence in the present study. It was noted by Greicius that this default mode network was not associated with the alpha generating system, as its activity remained unchanged when subjects opened their eyes. Beckmann et al. (2005) found ten independent resting topographic patterns, eight of which had pronounced left–right symmetry; Luca et al. (2006) and van de Ven et al. (2004) found similar patterns as well.

Two particularly relevant studies of brain connectivity in the resting state are those of Salvador et al. (2005) and Mantini et al. (2007). Their methodologies for identifying related areas are quite different, yet there is a notable degree of similarity in the results obtained. Salvador et al. (2005) uses pairwise correlations between the time series of regional activations to identify 76 pairs of regions [comprising 66 of 90 regions (73% of the regions)] with significant connectivity. Hierarchical cluster analysis was then used to separate the 66 anatomical regions into six groups. The regional networks found by Mantini et al. (2007) are based on segregation of time series of activations by independent component analysis (ICA) followed by correlation with the ICA time series to partition a subset of anatomical regions into six networks (it is not stated what fraction of the observed voxels are included in the networks, but it appears to be less than 50%). A comparison of the anatomical maps provided by Salvador et al. (2005) and Mantini et al. (2007) shows that each of five of the localized RSN in Mantini et al. (2007) are contained within in a single group given by Salvador et al. (2005): RSN 2 in Parietal-(pre)Motor, RSN 3 in Occipital, RSN 4 in Temporal, RSN 5 in Parietal-(pre)Motor, and RSN 6 in Frontal(c). Given this concordance in anatomical results between the two fMRI studies, we take as an initial point for the comparison with our results the correspondence between the RSN/groups and the topographic features found in EEG measures which define complexes of coherence pairs. They are each derived from values which measure relations which are relatively stable over a period of minutes, although there are almost certainly fluctuations of coherence or correlation when considering shorter time sequences within the total recording. Thus, we anticipate there to be some correspondence between the topographies in the different studies.

Our results are consistent with those obtained by Salvador et al. (2005). In Salvador et al. (2005), the 76 significant correlation results taken from the 4,005 possible correspond to the entire set of our coherence results, since we have omitted those coherence pairs with low values. Of first importance in Salvador et al. (2005) is the correlation of significantly large number of bilaterally symmetric locations (15 of the largest 20 correlations) and extremely few diagonally oriented locations, which corresponds to the primary topographical pattern in our selected coherence pairs. Second, in Salvador et al. (2005), the pattern exhibited in the MDS map is that one of the two axes has an anterior–posterior gradient, and the other, considering cortical regions only, has a temporal to midline gradient. The same axial orientation is present in our theta and alpha band MDS maps of coherence, illustrated in Fig. 13. This suggests that the same neurophysiological factors underlie both theta and alpha EEG coherence and the low frequency correlation in hemodynamic activity; possibly properties of thalamocortical circuits.

Our results have an interesting correspondence with those obtained by Mantini et al. 2007. Mantini et al. (2007) not only determines localized networks, but also provides correlations between the time series associated with each RSN (not the time series associated with the marked areas of each RSN) and the overall time series of EEG spectral power. This blurs the association of the RSN and the EEG characteristics associated with it, so that the use of these correlations to match RSN and EEG coherence topography is limited. There is some degree of coincidence between the RSN topography and coherence topography. We may point to the correspondence between theta coherence and the negative temporal activations found in RSN 4, alpha coherence and the negative occipital activations found in RSNs 2 and 3, and beta coherence and positive midline activations found in RSNs 1 and 6. This suggests the hypothesis that the activity in each network is predominantly in a distinct frequency band. That the time courses of the BOLD activity in networks have correlations with the time courses of the power in several EEG frequency bands does not contradict this hypothesis. The time courses of the EEG power used by Mantini et al. (2007) are for the entire scalp and are not site-specific. In order to investigate the hypothesis of the frequency specificity of RSN's, the complexes of scalp recording sites indicated by the topography of the networks could be checked for correlated neural activity. Comparisons with single-site data are not as effective, as at any one site scalp recordings may contain the activity from a number of the distinct networks operating at different frequencies. This is the case in our data, where the minimum value choice criterion of coherence pairs means that coherent activity is found at all frequencies in each pair. The presence of the banding leads us to attribute activity in different frequency bands to the action of different neurophysiological mechanisms. The spatial distribution of the neural structures underlying these mechanisms may vary considerably from one mechanism to another, as is suggested by our topographic results. On the other hand, it is certainly possible that there are cross-frequency relations which are not captured by the measures we have used. The presence of these relations would suggest more complex multi-frequential patterns in addition to those presented here.

A limitation of our study is that it examines connectivity on a single time scale, the four and quarter minutes over which the data were collected. Although this allows precise frequency estimation, it obscures patterns of temporal fluctuation which are undoubtedly present in the data (Breakspear et al. 2004; Koenig et al. 2005; Honey et al. 2007). Given the detail in which the frequency band structure has been determined, it may be worthwhile to reanalyze the data using alternative methods to determine the patterns of temporal fluctuation in coherence (Möller et al. 2001; Astolfi et al. 2008). This would produce values that are similar in structure to the time series used in the fMRI studies.

Our primary conclusion is that there are different mechanisms for coherent activity in different frequency bands. The variation of coherence across frequency and topography cannot be explained simply as the spatial variation of the parameters controlling a single mechanism. We are encouraged by the consistency between the topographic patterns revealed in our study and those found in fMRI and MEG studies. We regard our results as preliminary, as the use of a denser grid of electrodes, Laplacian as well as bipolar derivations, and specific phase information, would bring more detail to the topographical structure we have discerned in the data. This would aid in determining the sources of coherent activity measured by scalp EEG. Ultimately, the integration of the information from imaging and electrophysiological studies would serve to relate more clearly RSN to patterns in ongoing neural activity.

Acknowledgments We thank our present and former colleagues at the Henri Begleiter Neurodynamics Laboratory for their help in preparing this paper. We thank Jay Weedon for enlightening discussions of data analysis, as well as two anonymous reviewers whose comments and questions led to signficant improvements in this paper. We dedicate this paper to the memory of Henri Begleiter, who encouraged the first steps in its creation.

Appendix: location of coherence pairs

The table presents a classification of all pairs used in this study. Figures illustrating the scalp locations follow (see Tables 1, 2; Figs. 15, 16).

Table 1 Classification of coherence pairs

	Sagittally oriented coherence pairs		
	Symmetric	Midline	Non-midline
Frontal symmetric	FP2-F4–FP1-F3		
Frontal-central			
Adjacent	F4-C4–F3-C3	FZ-CZ–F3-C3	F3-C3–F7-T7
		FZ-CZ–F4-C4	F4-C4–F8-T8
Distant	F8-T8–F7-T7	FZ-CZ–F7-T7	F4-C4–F7-T7
		FZ-CZ–F8-T8	F3-C3–F8-T8
Central–parietal			
Adjacent	C4-P4–C3-P3	C3-P3–CZ-PZ	C3-P3–T7-P7
		C4-P4–CZ-PZ	C4-P4–T8-P8
Distant	T8-P8–T7-P7	T7-P7–CZ-PZ	C4-P4–T7-P7
		T8-P8–CZ-PZ	C3-P3–T8-P8
Parietal symmetric	P4-O2–P3-O1		

	Laterally oriented coherence pairs		
	Left	Right	Midline
Intrahemispheric	T7-C3–F7-F3	T8-C4–F8-F4	F3-FZ–CZ-C3
	P7-P3–F7-F3	P8-P4–F8-F4	FZ-F4–CZ-C4
	P7-P3–T7-C3	P8-P4–T8-C4	PZ-P3–CZ-C3
			PZ-P4–CZ-C4

	Symmetric	Diagonal
Interhemispheric	F8-F4–F7-F3	F8-F4–T7-C3
	T8-C4–T7-C3	F7-F3–T8-C4
	P8-P4–P7-P3	T8-C4–P7-P3
		T7-C3–P8-P4

Table 2 Distance between coherence pairs

Name	Distance (m)	Name	Distance (m)
Sagittally oriented coherence pairs		Laterally oriented coherence pairs	
F3-C3–F7-T7	0.079	T7-C3–F7-F3	0.085
F4-C4–F8-T8	0.079	P7-P3–T7-C3	0.085
C3-P3–T7-P7	0.079	T8-C4–F8-F4	0.085
C4-P4–T8-P8	0.079	P8-P4–T8-C4	0.085
FZ-CZ–F3-C3	0.088	F3-FZ–CZ-C3	0.089
FZ-CZ–F4-C4	0.088	FZ-F4–CZ-C4	0.089
C3-P3–CZ-PZ	0.088	PZ-P3–CZ-C3	0.089
C4-P4–CZ-PZ	0.088	PZ-P4–CZ-C4	0.089
FP2-F4–FP1-F3	0.126	P7-P3–F7-F3	0.171
P4-O2–P3-O1	0.126	P8-P4–F8-F4	0.171
FZ-CZ–F7-T7	0.166	F8-F4–F7-F3	0.207
FZ-CZ–F8-T8	0.166	P8-P4–P7-P3	0.207
T7-P7–CZ-PZ	0.166	T7-C3–F8-F4	0.260
T8-P8–CZ-PZ	0.166	T8-C4–F7-F3	0.260
F4-C4–F3-C3	0.177	P7-P3–T8-C4	0.260
C4-P4–C3-P3	0.177	P8-P4–T7-C3	0.260
F4-C4–F7-T7	0.253	T8-C4–T7-C3	0.270
F3-C3–F8-T8	0.253		
C4-P4–T7-P7	0.253		
C3-P3–T8-P8	0.253		
F8-T8–F7-T7	0.321		
T8-P8–T7-P7	0.321		

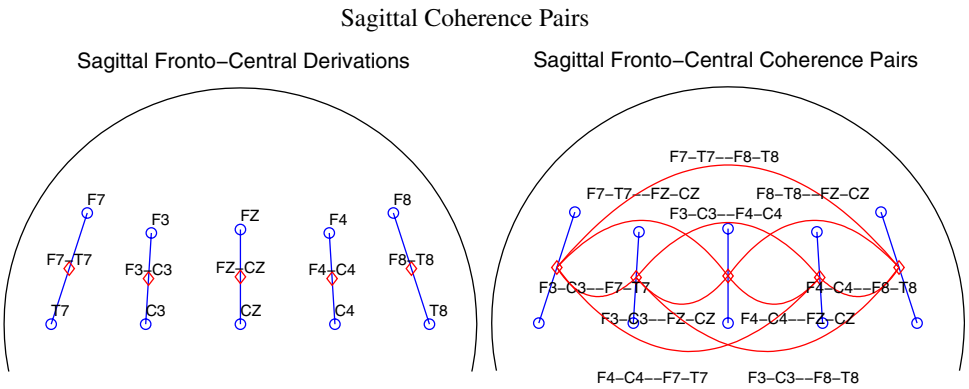

Fig. 15 *Left panel*, fronto-central electrodes and sagittal bipolar derivations. *Right panel*, *red lines* connect midpoints of coherence pairs for all pairs calculations. Central–parietal is similar. Frontal and occipital pairs not illustrated

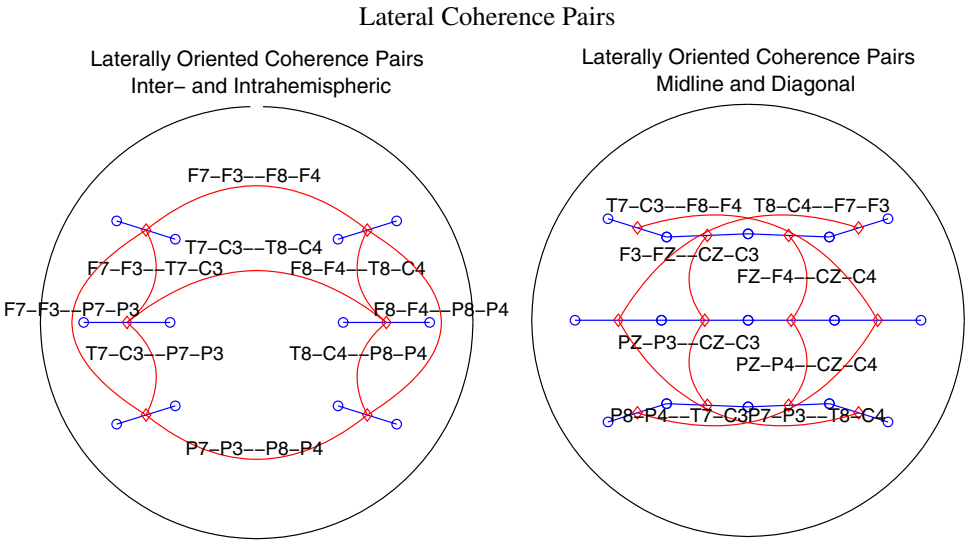

Fig. 16 *Left panel* derivations and coherence pairs for lateral intrahemispheric and interhemispheric coherence pairs. *Right panel* derivations and coherence pairs for lateral midline and diagonal coherence pairs

References

Astolfi L, Cincotti F, Mattia D, De Vico Fallani F, Tocci A, Colosimo A, Salinari S, Marciani MG, Hesse W, Witte H, Ursino M, Zavaglia M, Babiloni F (2008) Tracking the time-varying cortical connectivity patterns by adaptive multivariate estimators. IEEE Trans Biomed Eng 55(3):902–913

Babiloni F, Babiloni C, Fattorini L, Carducci F, Onorati P, Urbano A (1995) Performances of surface Laplacian estimators: a study of simulated and real scalp potential distributions. Brain Topogr 8(1):35–45

Beckmann CF, DeLuca M, Devlin JT, Smith SM (2005) Investigations into resting-state connectivity using independent component analysis. Philos Trans R Soc Lond B Biol Sci 360(1457):1001–1013

Bendat J, Piersol A (1971) Random data: analysis and measurement procedures. Wiley, New York

Breakspear M, Terry JR (2002) Topographic organization of nonlinear interdependence in multichannel human EEG. Neuroimage 16(3 Pt 1):822–835

Breakspear M, Williams LM, Stam CJ (2004) A novel method for the topographic analysis of neural activity reveals formation and dissolution of 'dynamic cell assemblies'. J Comput Neurosci 16(1):49–68

Bruce A, Gao H (1994) S+ wavelets user's manual. Mathsoft Inc., Seattle

Buzsáki G, Draguhn A (2004) Neuronal oscillations in cortical networks. Science 304(5679):1926–1929

Cantero JL, Atienza M, Salas RM (2002) Human alpha oscillations in wakefulness, drowsiness period, and REM sleep: different electroencephalographic phenomena within the alpha band. Neurophysiol Clin 32(1):54–71

Chorlian DB, Tang Y, Rangaswamy M, O'Connor S, Rohrbaugh J, Taylor R, Porjesz B (2007) Heritability of EEG coherence in a large sib-pair population. Biol Psychol 75(3):260–266

Cover KS, Stam CJ, van Dijk BW (2004) Detection of very high correlation in the alpha band between temporal regions of the human brain using MEG. Neuroimage 22(4):1432–1437

David O, Friston KJ (2003) A neural mass model for MEG/EEG: coupling and neuronal dynamics. Neuroimage 20(3):1743–1755

De Luca M, Beckmann CF, De Stefano N, Matthews PM, Smith SM (2006) fMRI resting state networks define distinct modes of long-distance interactions in the human brain. Neuroimage 29(4):1359–1367

Durbin J, Watson GS (1950) Testing for serial correlation in least squares regression, I. Biometrika 37:409–428

Durbin J, Watson GS (1951) Testing for serial correlation in least squares regression, II. Biometrika 38 :159–179

Feige B, Scheffler K, Esposito F, Di Salle F, Hennig J, Seifritz E (2005) Cortical and subcortical correlates of electroencephalographic alpha rhythm modulation. J Neurophysiol 93(5):2864–2872

Feshchenko VA, Reinsel RA, Veselis RA (2001) Multiplicity of the alpha rhythm in normal humans. J Clin Neurophysiol 18(4):331–344

Fox MD, Raichle ME (2007) Spontaneous fluctuations in brain activity observed with functional magnetic resonance imaging. Nat Rev Neurosci 8(9):700–711

Fox MD, Snyder AZ, Vincent JL, Raichle ME (2007) Intrinsic fluctuations within cortical systems account for intertrial variability in human behavior. Neuron 56(1):171–184

Fries P, (2005) A mechanism for cognitive dynamics: neuronal communication through neuronal coherence. Trends Cogn Sci 9(10):474–480

Gasser T, Sroka L, Mocks J (1985) The transfer of EOG activity into the EEG for eyes open and closed. Electroencephalogr Clin Neurophysiol 61: 181–193

Gasser T, Sroka L, Mocks J (1986) The correction of EOG artifacts by frequency dependent and frequency independent methods. Psychophysiology 23:704–712

Goldman RI, Stern JM, Engel J Jr, Cohen MS (2002) Simultaneous EEG and fMRI of the alpha rhythm. Neuroreport 13(18):2487–2492

Greicius MD, Krasnow B, Reiss AL, Menon V (2003) Functional connectivity in the resting brain: a network analysis of the default mode hypothesis. Proc Natl Acad Sci USA 100(1):253–258

Grieve PG, Emerson RG, Fifer WP, Isler JR, Stark RI (2003) Spatial correlation of the infant and adult electroencephalogram. Clin Neurophysiol 114(9):1594–1608

Hagmann P, Cammoun L, Gigandet X, Meuli R, Honey CJ, Wedeen VJ, Sporns O (2008) Mapping the structural core of human cerebral cortex. PLoS Biol 6(7):e159

Hamming R (1983) Digital filters. Prentice, Englewood Cliffs

Hanslmayr S, Aslan A, Staudigl T, Klimesch W, Herrmann CS, Bäuml KH Prestimulus oscillations predict visual perception performance between and within subjects. Neuroimage 37(4):1465–1473

Honey CJ, Kötter R, Breakspear M, Sporns O (2007) Network structure of cerebral cortex shapes functional connectivity on multiple time scales. Proc Natl Acad Sci USA 104(24):10240–10245

Hughes SW, Crunelli V (2005) Thalamic mechanisms of EEG alpha rhythms and their pathological implications. Neuroscientist 11(4):357–372

Hughes JR, John ER (1999) Conventional and quantitative electroencephalography in psychiatry. J Neuropsychiatry Clin Neurosci 11(2):190–208

Kaminski M, Ding M, Truccolo WA, Bressler SL (2001) Evaluating causal relations in neural systems: granger causality, directed transfer function and statistical assessment of significance. Biol Cybern 85(2):145–157

Karameh FN, Dahleh MA, Brown EN, Massaquoi SG (2006) Modeling the contribution of lamina 5 neuronal and network dynamics to low frequency EEG phenomena. Biol Cybern 95(4):289–310

Koenig T, Studer D, Hubl D, Melie L, Strik WK (2005) Brain connectivity at different time-scales measured with EEG. Philos Trans R Soc Lond B Biol Sci 360(1457):1015–1023

Laufs H, Kleinschmidt A, Beyerle A, Eger E, Salek-Haddadi A, Preibisch C, Krakow K (2003) EEG-correlated fMRI of human alpha activity. Neuroimage 19(4):1463–1476

Laufs H, Krakow K, Sterzer P, Eger E, Beyerle A, Salek-Haddadi A, Kleinschmidt A (2003) Electroencephalographic signatures of attentional and cognitive default modes in spontaneous brain activity fluctuations at rest. Proc Natl Acad Sci USA 100(19):11053–11058

Laufs H, Holt JL, Elfont R, Krams M, Paul JS, Krakow K, Kleinschmidt A (2006) Where the BOLD signal goes when alpha EEG leaves. Neuroimage 31(4):1408–1418

Möller E, Schack B, Arnold M, Witte H (2001) Instantaneous multivariate EEG coherence analysis by means of adaptive high-dimensional autoregressive models. J Neurosci Methods 105(2):143–158

Mantini D, Perrucci MG, Del Gratta C, Romani GL, Corbetta M (2007) Electrophysiological signatures of resting state networks in the human brain. Proc Natl Acad Sci USA 104(32):13170–13175

Marple SL (1987) Digital spectral analysis. Prentice Hall, Englewood Cliffs

Moosmann M, Ritter P, Krastel I, Brink A, Thees S, Blankenburg F, Taskin B, Obrig H, Villringer A (2003) Correlates of alpha rhythm in functional magnetic resonance imaging and near infrared spectroscopy. Neuroimage 20(1):145–158

Murias M, Swanson JM, Srinivasan R (2007) Functional connectivity of frontal cortex in healthy and ADHD children reflected in EEG coherence. Cereb Cortex 17(8):1788–1799

Murias M, Webb SJ, Greenson J, Dawson G (2007) Resting state cortical connectivity reflected in EEG coherence in individuals with autism. Biol Psychiatry 62(3):270–273

Nunez PL, Srinivasan R, Westdorp AF, Wijesinghe RS, Tucker DM, Silberstein RB, Cadusch PJ (1997) EEG coherency. I: statistics, reference electrode, volume conduction, Laplacians, cortical imaging, and interpretation at multiple scales. Clin Neurophysiol 103:499–515

Nunez PL, Silberstein RB, Shi Z, Carpenter MR, Srinivasan R, Tucker DM, Doran SM, Cadusch PJ, Wijesinghe RS (1999) EEG coherency II: experimental comparisons of multiple measures. Clin Neurophysiol 110(3):469–486

Nunez PL, Silberstein RB (2000) On the relationship of synaptic activity to macroscopic measurements: does co-registration of EEG with fMRI make sense? Brain Topogr 13(2):79–96

Nunez PL, Srinivasan R (2006) A theoretical basis for standing and traveling brain waves measured with human EEG with implications for an integrated consciousness. Clin Neurophysiol 117(11):2424–2435

Nunez PL, Wingeier BM, Silberstein RB (2001) Spatial–temporal structures of human alpha rhythms: theory, microcurrent sources, multiscale measurements, and global binding of local networks. Hum Brain Mapp 13(3):125–164

O'Connor SC, Robinson PA (2004) Spatially uniform and nonuniform analyses of electroencephalographic dynamics, with application to the topography of the alpha rhythm. Phys Rev E Stat Nonlin Soft Matter Phys70(1 Pt 1):011911

Porjesz B, Almasy L, Edenberg HJ, Wang K, Chorlian DB, Foroud T, Goate A, Rice JP, O'Connor SJ, Rohrbaugh J, Kuperman S, Bauer LO, Crowe RR, Schuckit MA, Hesselbrock V, Conneally PM, Tischfield JA, Li TK, Reich T, Begleiter H (2002) Linkage disequilibrium between the beta frequency of the human EEG and a GABAA receptor gene locus. Proc Natl Acad Sci USA 99(6):3729–3733

Raichle ME, Gusnard DA (2005) Intrinsic brain activity sets the stage for expression of motivated behavior. J Comp Neurol 493(1):167–176

Raichle ME, Snyder AZ (2007) A default mode of brain function: a brief history of an evolving idea. Neuroimage 37(4):1083–1090

Rangaswamy M, Porjesz B, Chorlian DB, Wang K, Jones KA, Bauer LO, Rohrbaugh J, O'Connor SJ, Kuperman S, Reich T, Begleiter H (2002) Beta power in the EEG of alcoholics. Biol Psychiatry 52(8):831–842

Rangaswamy M, Porjesz B, Chorlian DB, Choi K, Jones KA, Wang K, Rohrbaugh J, O'Connor S, Kuperman S, Reich T, Begleiter H

(2003) Theta power in the EEG of alcoholics. Alcohol Clin Exp Res 27(4):607–615

Rangaswamy M, Porjesz B, Chorlian DB, Wang K, Jones KA, Kuperman S, Rohrbaugh J, O'Connor SJ, Bauer LO, Reich T, Begleiter H (2004) Resting EEG in offspring of male alcoholics: beta frequencies. Int J Psychophysiol 51(3):239–251

Robinson PA (2003) Neurophysical theory of coherence and correlations of electroencephalographic and electrocorticographic signals. J Theor Biol 222(2):163–175

Robinson PA, Rennie CJ, Rowe DL, O'Connor SC, Wright JJ, Gordon E, Whitehouse RW (2003) Neurophysical modeling of brain dynamics. Neuropsychopharmacology 28(Suppl 1):S74–S79

Robinson PA (2005) Propagator theory of brain dynamics. Phys Rev E Stat Nonlin Soft Matter Phys 72(1 Pt 1):011904

Salvador R, Suckling J, Coleman MR, Pickard JD, Menon D, Bullmore E (2005) Neurophysiological architecture of functional magnetic resonance images of human brain. Cereb Cortex 15(9):1332–1342

Sarnthein J, Morel A, von Stein A, Jeanmonod D (2005) Thalamocortical theta coherence in neurological patients at rest and during a working memory task. Int J Psychophysiol 57(2):87–96

Sarnthein J, Jeanmonod D (2007) High thalamocortical theta coherence in patients with Parkinson's disease. J Neurosci 27(1):124–131

Schreckenberger M, Lange-Asschenfeldt C, Lochmann M, Mann K, Siessmeier T, Buchholz HG, Bartenstein P, Grunder G (2004) The thalamus as the generator and modulator of EEG alpha rhythm: a combined PET/EEG study with lorazepam challenge in humans. Neuroimage 22(2):637–644

Srinivasan R, Nunez PL, Silberstein RB (1998) Spatial filtering and neocortical dynamics: estimates of EEG coherence. IEEE Trans Biomed Eng 45(7):814–826

Srinivasan R (1999) Spatial structure of the human alpha rhythm: global correlation in adults and local correlation in children. Clin Neurophysiol 110(8):1351–1362

Srinivasan R, Winter WR, Nunez PL (2006) Source analysis of EEG oscillations using high-resolution EEG and MEG. Prog Brain Res 159:29–42

Srinivasan R, Winter WR, Ding J, Nunez PL (2007) EEG and MEG coherence: measures of functional connectivity at distinct spatial scales of neocortical dynamics. J Neurosci Methods 166(1):41–52

Steyn-Ross ML, Steyn-Ross DA, Wilson MT, Sleigh JW (2007) Gap junctions mediate large-scale Turing structures in a mean-field cortex driven by subcortical noise. Phys Rev E Stat Nonlin Soft Matter Phys 76(1 Pt 1):011916

Strang G, Nguyen T (1996) Wavelets and filter banks. Wellesley-Cambridge Press, Wellesley

Tang Y, Chorlian DB, Rangaswamy M, O'Connor S, Taylor R, Rohrbaugh J, Porjesz B, Begleiter H (2007) Heritability of bipolar EEG spectra in a large sib-pair population. Behav Genet 37(2):302–313

Tang Y, Chorlian DB, Rangaswamy M, Porjesz B, Bauer L, Kuperman S, O'Connor S, Rohrbaugh J, Schuckit M, Stimus A, Begleiter H (2007) Genetic influences on bipolar EEG power spectra. Int J Psychophysiol 65(1):2–9

Tenenbaum JB, de Silva V, Langford JC (2000) A global geometric framework for nonlinear dimensionality reduction. Science 290 (5500):2319–2323

Thatcher RW, Krause PJ, Hrybyk M (1986) Cortico-cortical associations and EEG coherence: a two-compartmental model. Electroencephalogr Clin Neurophysiol 64(2):123–143

van de Ven VG, Formisano E, Prvulovic D, Roeder CH, Linden DE (2004) Functional connectivity as revealed by spatial independent component analysis of fMRI measurements during rest. Hum Brain Mapp 22(3):165–178

Ursino M, Zavaglia M (2007) Modeling analysis of the relationship between EEG rhythms and connectivity among different neural populations. J Integr Neurosci 6(4):597–623

von Stein A, Sarnthein J (2000) Different frequencies for different scales of cortical integration: from local gamma to long range alpha/theta synchronization. Intl J Psychophysiol 38:301–313

Wang K, Begleiter H (1999) Local polynomial estimate of surface Laplacian. Brain Topogr 12(1):19–29

Wang SY, Tang MX (2004) Exact confidence interval for magnitude-squared coherence estimates. IEEE Signal Process Lett 11(3):326–329

Zavaglia M, Astolfi L, Babiloni F, Ursino M (2008) The effect of connectivity on EEG rhythms, power spectral density and coherence among coupled neural populations: analysis with a neural mass model. IEEE Trans Biomed Eng 55(1):69–77